Correspondence

Esaki Diode Oscillators from 3 to 40 KMC*

Esaki diode oscillators operating at microwave frequencies of 10 kmc and below have been reported in the literature.[1–5] Fundamental power up to 40 kmc in frequency has now been obtained from Esaki diode oscillators, with appreciable harmonic output to about 63 kmc. The microwave power at all wavelengths has been sufficient to be detected and displayed by the simplest video methods. Although small-area junction diodes of both gallium arsenide and germanium have provided substantial power below 10 kmc, the highest frequencies were obtained with gallium-arsenide units.

Junctions were formed by alloying tin to zinc-diffused gallium arsenide, and aluminum to germanium doped with arsenic. Alloying took place when an electric current was passed through a point of the appropriate metal which had been brought in contact with the semiconductor. Peak currents of the resulting Esaki diodes ranged from less than 100 μa to more than 30 ma, depending upon the forming conditions. Peak-to-valley current ratios exceeded 2:1 and were commonly 6:1. The impurity concentration in the germanium was approximately 6×10^{19}, and, although the carrier concentration in the gallium arsenide was not measured, the resistivity was 0.0015 ohm-cm.

Fig. 1(a) shows the current-voltage characteristic of a gallium-arsenide Esaki diode in an oscillating circuit. The *s*-shaped deviation from the expected static characteristic indicates oscillation. Except for the voltage scale, this characteristic was typical of those obtained with germanium as well as with gallium arsenide.

Oscillations ranging in frequency from 2.7 to 33.4 kmc have been obtained in cylindrical cavities. A diode of either gallium arsenide or germanium shunted each cavity at the apex of a re-entrant cone, as shown in Fig. 2. The cavity resonances occurred at frequencies for which the radius equaled approximately an odd integral number of quarter wavelengths, altered by the diode loading. The circuit of Fig. 2 is resonant near odd-order harmonics, and power at these frequencies was coupled out of the cavity through the loop. Odd harmonics through the seventh have easily been detected from a germanium unit having a fundamental frequency of 2.7 kmc. Low-order harmonics of much higher fundamental frequencies

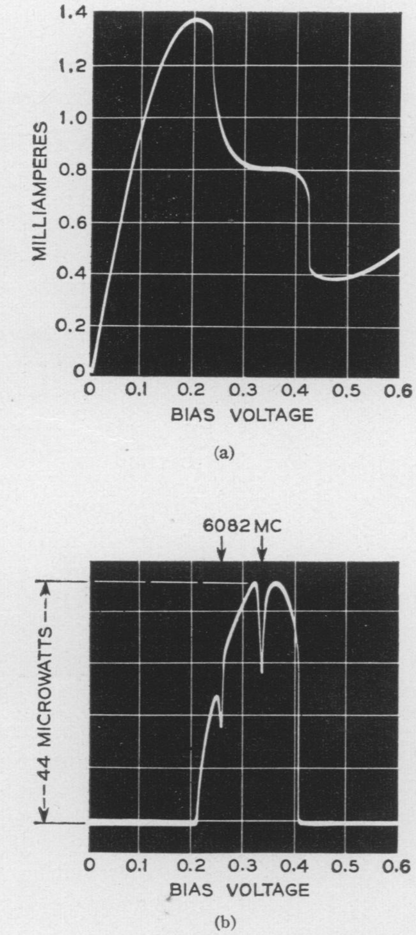

Fig. 1—(a) Current-voltage characteristic of a gallium-arsenide Esaki diode oscillating at 6 kmc in a cavity. (b) Detected power output from the cavity oscillator. The sharp dips are absorptions from a wavemeter set to 6082 mc.

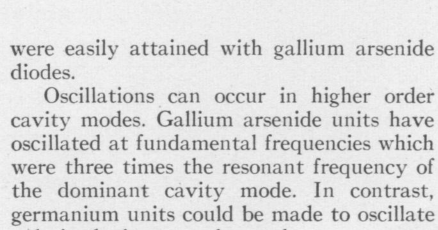

Fig. 2—Section of a cavity oscillator.

were easily attained with gallium arsenide diodes.

Oscillations can occur in higher order cavity modes. Gallium arsenide units have oscillated at fundamental frequencies which were three times the resonant frequency of the dominant cavity mode. In contrast, germanium units could be made to oscillate only in the lowest-order mode.

Fundamental oscillation in a higher-order cavity mode can be confused with a harmonic of an oscillation in the lowest-order mode, since adjustments in the coupling loop and external loading can shift operation from one mode to the other. A ferrimagnetic resonance phenomenon was employed to differentiate between these possibilities. A small yttrium iron garnet sphere was placed within the cavity diametrically opposite the coupling loop, and was biased with an external magnetic field along the axis of the cavity. With fields near resonance at either a fundamental or a low-order harmonic present within the cavity, the output was altered drastically in power and frequency. Thus, the fundamental frequency of oscillation could be inferred from the magnetic field and the known relationship between magnetic field and frequency for the sphere.

Waveguide circuits consisted of gallium-arsenide diodes mounted directly across the center of relatively low impedance waveguide, with a movable piston in one end of the waveguide. Oscillations were readily obtained with the other end of the waveguide feeding directly into a detector, or into an isolator or attenuator. The fundamental frequencies were often three or four times the waveguide cutoff frequencies.

The circuit operation of Esaki diodes may be classified somewhat arbitrarily as either weakly or strongly oscillating. The static characteristics of both kinds of operation show an *s*-shaped oscillatory region which, for weakly oscillating circuits, is less pronounced and extends over a smaller bias range than for strong oscillators. Fundamental microwave power has been observed at frequencies from 14.5 to 39.9 kmc in various weakly oscillating circuits, using diodes having peak currents in the 300–700-μamp range. The maximum power measured was 3.5 μw in the 17–25-kmc region, falling off to about 0.2 μw at 37 kmc. Movement of the piston behind the diode could be used to tune the frequency of a given circuit 300 to 500 mc, or to suppress the oscillation. Diodes having peak currents from 1 to 3 ma oscillated more strongly in the same circuits, and the oscillations were less readily controlled by the piston. Fundamental frequencies of high-current diode oscillators were, in general, not as high as those for lower-current units operating in the same circuits. The maximum fundamental power observed with strongly oscillating circuits was 50 μw at 16.7 kmc. Appreciable harmonic output was observed at frequencies to 62.7 kmc, where the SNR of the detected output displayed on an oscilloscope was as high as 20:1.

Because both the negative resistance and capacitance of a diode varies with voltage, the frequency of oscillation depends somewhat upon bias, and the voltage tuning range may be as much as several per cent of the center frequency. As the bias voltage is increased, the frequency of weakly oscillating circuits decreases monotonically. For large amplitudes of oscillation, however, the frequency may go through a minimum or maximum or both. Fig. 1(b) shows the

* Received by the IRE, July 14, 1960.

[1] H. S. Sommers, Jr., "Tunnel diodes as high frequency devices," Proc. IRE, vol. 47, pp. 1201–1206; July, 1959.

[2] R. F. Rutz, "A 3000-mc lumped parameter oscillator using an Esaki negative-resistance diode," *IBM J. Res. & Dev.*, vol. 3, pp. 372–374; October, 1959.

[3] R. N. Hall, "Tunnel diodes," IRE Trans. on Electron Devices, vol. ED-7, pp. 1–9; January, 1960.

[4] R. L. Batdorf, G. C. Dacey, R. L. Wallace, and D. J. Walsh, "Esaki diode in InSb," *J. Appl. Phys.* vol. 31, pp. 613–614; March, 1960.

[5] J. K. Pulfer, "Voltage tuning in tunnel diode oscillators," Proc. IRE, vol. 48, p. 1155; June, 1960.

detected power output of the diode of Fig. 1(a) and is an example of a strongly oscillating circuit. The two sharp dips in power are absorptions by a wavemeter at 6082 mc. The peak power output was 44 microwatts with an efficiency of 15 per cent.

Very strongly oscillating circuits are much more complicated in behavior, and are characteristic of high peak-current units. Deviations from the non-oscillating characteristic curves are no longer s-shaped, but show multiple breaks which are accompanied by a power output very different in shape from a parabola. The frequency behavior is far from simple, and the harmonic content is strong enough to give sizable power output well into the millimeter wavelength region.

We found the performance of gallium-arsenide diodes to be superior at high frequencies to that of diodes made from the most highly doped germanium available to us. Gallium-arsenide diodes loaded a cavity resonant at 4 kmc almost imperceptibly, but the best germanium units in the same circuit oscillated barely in excess of 2.8 kmc. The higher fundamental frequencies and harmonics have been obtained with gallium-arsenide units. It appears that these gallium-arsenide diodes have a lower barrier capacitance than germanium units of the same negative resistance, and show promise for application in amplifiers and oscillators well into the millimeter wavelength regions.

Although the circuits employed here are probably far from optimum, high-frequency microwave power sufficient for certain applications has been generated at relatively high efficiencies with Esaki diodes. Power as low as 50 μw can be used, if necessary, for a local oscillator in heterodyne detection, and even less power will suffice for simple microwave measurements. As an illustration, Fig. 3 shows an oscilloscope display of the detected output of a frequency swept Esaki diode oscillator in waveguide having a peak power of about 0.2 μw; the absorption dip at 36.85 kmc is the ferrimagnetic resonance curve of an yttrium iron garnet sphere.

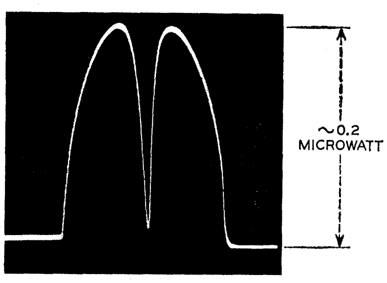

Fig. 3—Detected output of a frequency swept Esaki diode oscillator in waveguide. The peak power was about 0.2 μw. The absorption dip is the ferrimagnetic resonance curve of a YIG sphere at 36.85 kmc, and the frequency range covered was 120 mc.

We should like to thank W. M. Sharpless for helpful discussions.

R. Trambarulo
C. A. Burrus
Bell Telephone Labs.
Holmdel, N. J.

The Emitter Diffusion Capacitance of Drift Transistors*

The emitter diffusion capacitance of drift transistors with exponential impurity distributions was calculated by Krömer[1] for high built-in fields as:

$$C_{DE} = \frac{qI_E}{kT}\frac{W^2}{D}\frac{1}{\eta^2} \tag{1}$$

where:

I_E = emitter current,

kT/q = thermal voltage,

W = base width,

D = diffusion constant of minority carriers (holes),

$$\eta = \frac{q}{kT}E_bW = \ln\left(\frac{\text{impurity conc. at the emitter}}{\text{impurity conc. at } W}\right),$$

E_b = built-in field.

For convenience, p-n-p transistors are considered.

Eq. (1) was obtained by solving the input admittance, y_{11}, for low frequencies and high η. In an attempt to calculate the diffusion capacitance in the common base configuration

$$C_{DE} = \frac{dQ}{dV_E} \tag{2}$$

we shall use the integrated hole concentration as the stored charge Q. The hole distribution may be obtained from the expression for the hole current density:

$$J = q\mu E_b P - qD\frac{dP}{dx} \tag{3}$$

where μ=mobility of holes, P=the hole concentration.

The solution of (3) leads to:

$$P = \frac{JW}{qD}\frac{1-\exp\left[-\eta\left(1-\frac{x}{W}\right)\right]}{\eta} = P_{EO}\frac{1-\exp\left[-\eta\left(1-\frac{x}{W}\right)\right]}{\eta} \tag{4}$$

where P_{EO} is the concentration of holes at the emitter in the diffusion transistor. The total stored charge is obtained as:

$$Q = qA\int_0^W Pdx = \frac{W^2}{D}I_E\frac{\eta-1+e^{-\eta}}{\eta^2}. \tag{5}$$

Using this charge in (2) (neglecting the equilibrium concentration and volume recombination), and considering that $dI_E/dV_E = qI_E/kT$ is independent of η, we obtain:

$$C_D = \frac{qI_E}{kT}\frac{W^2}{D}\frac{\eta-1+e^{-\eta}}{\eta^2}. \tag{6}$$

Eq. (6) gives the correct results for the diffusion transistor (η=0):

$$C_{DE}\ (\text{diffusion}) = \frac{qI_E}{kT}\frac{W^2}{2D}. \tag{7}$$

However, for large built-in fields (large η), (6) results in a $1/\eta$ dependence instead of the $1/\eta^2$ dependence obtained from y_{11}, *i.e.*, (1).

The discrepancy between the diffusion capacitance derived from the total stored charge, (6), and the diffusion capacitance derived from the emitter admittance, (1), is resolved by multiplying the emitter current in (6) by a factor Γ. The factor equals the ratio of the diffusion current by holes averaged over the base layer divided by the total hole current, *i.e.*,

$$\Gamma = \frac{I_E\ (\text{average diffusion})}{I_E\ (\text{total})}.$$

The average diffusion current over the base region is $qADP_E/W$, and the total current may be obtained from (3). Γ may then be written as:

$$\Gamma = \frac{P_E/W}{\eta P_E/W + (-P')_{X=0}} = \frac{P_E}{\eta P_E + P_{EO}e^{-\eta}} \tag{8}$$

where $P'(x=0)$ has been substituted from (4), and P_E is the concentration of holes at the emitter for any η. From (4) we may write:

$$P_E = P_{EO}\frac{1-e^{-\eta}}{\eta}. \tag{9}$$

Setting (9) into (8):

$$\Gamma = \frac{1-e^{-\eta}}{\eta}. \tag{10}$$

The necessity of multiplying by this factor can be interpreted by saying that only the diffusion current of holes contributes to the diffusion capacitance. In other words, only the stored charges carried by diffusion can be reclaimed by the emitter lead. This may also be seen if we write the input admittance

$$\left(\frac{\partial I_E}{\partial V_E}\right)_{V_C=0} = \frac{\partial}{\partial V_E}(\text{drift current } (x=0) + \text{diffusion current } (x=0)).$$

Since the drift term depends only on the emitter boundary of the base region, the term will remain real and will not contribute to the diffusion capacitance.

The emitter diffusion capacitance in the common base configuration, C_{DE}, is therefore ΓC_D, or

$$C_{DE} = \frac{qI_E}{kT}\frac{W^2}{D}\left(\frac{\eta-1+e^{-\eta}}{\eta^2}\cdot\frac{1-e^{-\eta}}{\eta}\right). \tag{11}$$

For η=0 this expression returns to the diffusion transistor case in (7). For large η it gives the correct $1/\eta^2$ dependence. Fig. 1 shows the variance of the factor in parentheses with η.

Measurement of the diffusion capacitance supplies information about the built-in field of a drift transistor. Such a measurement is difficult in the common base configuration due to the small parallel resistance $\approx kT/qI_E$. In the common emitter configuration, however, the ohmic part is approximately $\beta_0 kT/qI_E$; where β_0 is the common emitter current amplification factor. Such a basic measuring circuit is shown in Fig. 2. In the case of diffusion transistors,

* Received by the IRE, July 5, 1960.
[1] H. Krömer, "The Drift Transistor"; *Transistors I*, RCA Labs., Princeton, N. J.; 1956.

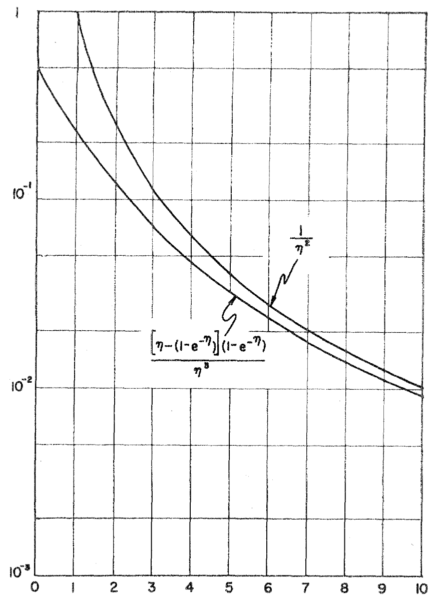

Fig. 1—The factor appearing in the emitter diffusion capacitance. Krömer's approximation by $1/\eta^2$ is also shown.

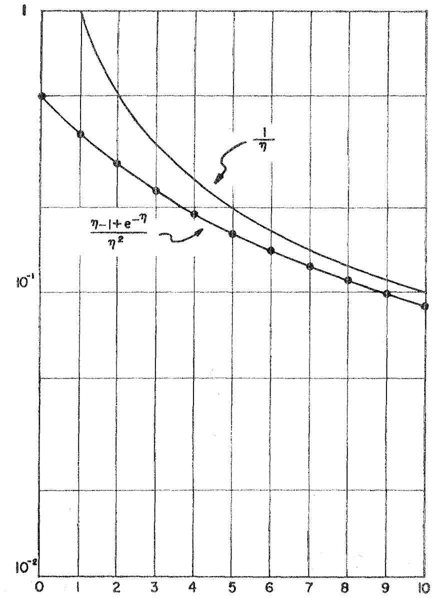

Fig. 3—The factor appearing in the measured capacitance. A $1/\eta$ approximation is also shown.

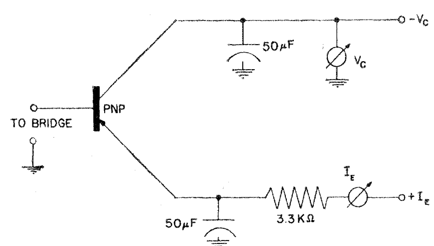

Fig. 2—Circuit for measurement of the diffusion capacitance in common emitter. Bridge provides the bias path for the base.

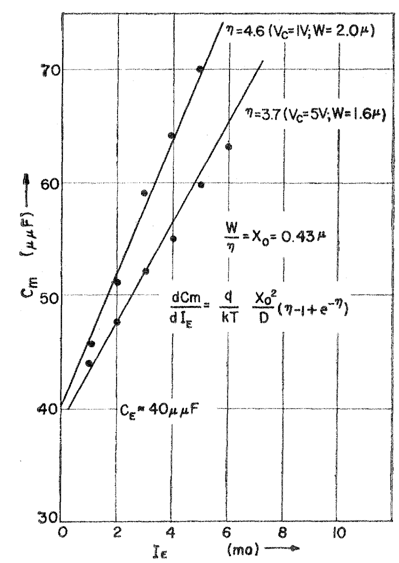

Fig. 4—Measured input capacitance for a p-n-p drift transistor for two collector voltages. The measured points are indicated by dots and the calculated slopes are drawn through them. C_E is the depletion layer capacitance.

the capacitance measured in this manner is C_{DE}. However, for drift transistors it will differ.

From four-pole theory, the input admittance in common emitter, y_{11E}, is:

$$y_{11E} = y_{11B} + y_{12B} + y_{21B} + y_{22B} \approx y_{11B} + y_{21B}. \quad (12)$$

y_{12B} and y_{22B} can be neglected, since they are much smaller than y_{21B} and y_{11B}. From (12) one can write:

$$y_{11Ei} = y_{11Bi} + y_{21Bi} \quad (13)$$

where the subscript i refers to the imaginary parts. Considering that

$$y_{21B} = -\alpha y_{11B} \quad (14)$$

where α is the current transport factor,

$$y_{21Bi} = \alpha_i y_{11Br} - y_{11Bi}\alpha_r \quad (15)$$

where the subscript $_r$ refers to the real part. Since $\alpha_r \approx 1$ for low frequencies, combining (13) and (15):

$$y_{11Ei} = \alpha_i y_{11Br} = \alpha_i \frac{qI_E}{kT}. \quad (16)$$

For low frequencies, the measured input capacitance in common emitter is then:

$$C_m = \frac{\alpha_i}{\omega}\frac{qI_E}{kT}. \quad (17)$$

Therefore, the capacitance which is measured is the imaginary part of the transport factor and not C_{DE}. By computing the imaginary part of the transport factor[2] for low frequencies and fitting an analytical expression to the result, we obtain

$$\frac{\alpha_i}{\omega}\frac{D}{W^2} = \frac{\eta - 1 + e^{-\eta}}{\eta^2}. \quad (18)$$

Therefore,

$$C_m = \frac{qI_E}{kT}\frac{W^2}{D}\left(\frac{\eta - 1 + e^{-\eta}}{\eta^2}\right). \quad (19)$$

[2] D. Thomas and J. Moll, "Junction transistor short-circuit current gain and phase determination," PROC. IRE, vol. 46, pp. 1177–1184; June, 1958. ($L = x_0$.)

Fig. 3 shows the factor in parentheses as a function of η. It also shows points computed from the full analytical expression for the alpha transfer function, [left-hand side of (18)], and a crude approximation by the factor $1/\eta$.

The capacitance *measured* in the common emitter configuration is the same as calculated for C_D in (6). This is expected if we consider that the emitter and collector leads are strapped together for ac in the common emitter configuration. In this case, for the δV_E change the total δQ (drift and diffusion components), can be reclaimed by the input terminals. Therefore $C_m = C_D$.

In the case of the diffusion transistor $C_m = C_{DE}$, but for drift transistors C_m is larger than C_{DE} by the factor $\eta/(1-e^{-\eta})$.

Fig. 4 shows the measured capacitance, C_m, for the p-n-p drift transistor with an impurity distribution closely resembling

$$N = N_0 \exp\left(-\frac{x}{x_0}\right) \quad (20)$$

with $x_0 = 0.43\ \mu$. The slopes expected from (19) agree with the measured values and justify the equation for C_m.

The authors are grateful for the advice of Dr. Kurt Lehovec of the Sprague Electric Company.

J. LINDMAYER
C. WRIGLEY
Sprague Electric Co.
North Adams, Mass.

Bomb-Excited "Whistlers"*

Theoretical and experimental studies of "whistler" or "magneto-ionic" modes, which allow the propagation of low-frequency electromagnetic waves through the ionosphere, have shown that these modes can be excited by lightning strokes[1] or by low-frequency radio transmitters.[2] In this note, we wish, first, to point out that these modes can also be excited by nuclear explosions, and second, to discuss some of the characteristics of the signals to be expected.

The information we require, relating to the electromagnetic characteristics of whistlers and of nuclear explosions, is all available in the unclassified literature.[1-3] The pertinent facts fall into two groups which describe the electromagnetic properties associated with the whistler modes and nuclear explosions, respectively.

Regarding the whistlers, it is known[1,2] that the propagation of electromagnetic waves through the ionosphere is qualitatively changed by the presence of the earth's magnetic field. If the earth's field were ab-

* Received by the IRE, May 31, 1960.
[1] R. O. Storey, "An investigation of whistling atmospherics," *Phil. Trans. Roy. Soc. (London) A*, vol. 246, pp. 113–141; July, 1953.
[2] R. A. Helliwell and E. Gehrels, "Observations of magneto-ionic duct propagation using man-made signals of very low frequency," PROC. IRE, vol. 46, pp. 785–787; April, 1958.
[3] J. C. Mark, "The detection of nuclear explosions," *Nucleonics*, vol. 17, pp. 64–73; August, 1959.

sent, electromagnetic waves of frequency lower than the plasma frequency would be totally reflected by the ionosphere. However, the earth's magnetic field introduces an anisotropy into an otherwise isotropic medium. This anisotropy has the effect of permitting the wave belonging to the extraordinary mode to penetrate the ionosphere, if the frequency is less than the gyrofrequency of the region. However, not all low-frequency waves are transmitted, but only those pulses, or wave-packets, that correspond to rays traveling at angles less than about 20° with the direction of the magnetic field. As a result, the low-frequency components of the wave-packet radiated by an impulsive disturbance move in a direction (the ray direction) that lies fairly close to the direction of a line of force of the earth's magnetic field.

The lateral spreading of the whistler mode structure is small; as a matter of practical experience, it is found[1] that lightning strokes will produce whistlers only when they occur within about 2000 km of the point of observation. Attenuation within the whistler mode is also small; measurements of the relation between the direct (ground-wave) signal produced by a radio transmitter and the signal produced by excitation of a whistler mode[2] have shown that propagation by the whistler mode is down only about 10 to 30 db from the direct signal. The signal received by the whistler mode is delayed about 1 second, since it propagates along a line of force of the earth's magnetic field. Finally, since the line of force passes much of the way through a dispersive medium, the original sharp pulse becomes diffuse, the component of frequency f arriving at a time proportional to $f^{-1/2}$.

Turning now to nuclear explosions, according to a recent account,[3] electromagnetic field strengths of tens of mv per meter have been recorded thousands of km from the burst point of a 1-kiloton bomb. The signal produced varies as the logarithm of the yield. At large distances, it is composed of low frequencies only, the high frequencies attenuating rapidly as the distance from the explosion increases.

Combining these two sets of facts, we conclude:

1) Nuclear explosions in the kiloton range can reasonably be expected to excite whistler modes. The corresponding electromagnetic signal propagates along a line of force of the earth's field, can penetrate the ionosphere, and consists of a pulse or wave-packet of low-frequency components dispersed according to the law that the time of arrival goes as $f^{-1/2}$. If the signal is sufficiently strong, pulses will be observed, caused by reflections of the wave at the points where the line of forces meets the surface of the earth. The successive pulses will be progressively more dispersed and their times of arrival will obey the integral relationships observed for whistlers.[1,2]
2) The whistler signal produced by a nuclear explosion will be localized in the neighborhood of the line of force along which the signal is propagating. The lateral spread about the line of force will be about 2000 km. Thus, on the surface of the earth, there will be two regions of detectability for each whistler, one where the line of force penetrates the earth near the burst point, and another at the conjugate point in the other hemisphere. The strength of the signal transmitted by the whistler mode will be about 10 to 30 db below the direct signal. Roughly, kiloton explosions will produce signals of hundredths or tenths of mv per meter at the conjugate point. The signal will be logarithmically dependent on the yield of the bomb.
3) A spherically symmetric system of charges and currents, in a spherically symmetric medium, cannot radiate electromagnetically because the electromagnetic field at large distances is a transverse, vector field and requires a unique direction of polarization to be defined, a condition that is incompatible with the assumed spherical symmetry of the sources and their surroundings. If, then, the earth's magnetic field is neglected, nuclear explosions can be expected to produce electromagnetic signals only at the top or the bottom of the atmosphere, where the properties of the medium change rapidly in a mean free path of the current-producing radiation emitted by the bomb. The middle region of the atmosphere, in particular, constitutes a "dead spot" for the generation of electromagnetic signals if the earth's field is ignored. Thus, we see that the anisotropy introduced by the earth's magnetic field has two effects. First, by impairing the spherical symmetry otherwise present in the middle atmosphere, it makes possible the generation of electromagnetic signals in this region, and this may explain why the signals observed from bursts in this region have not been as small as expected;[3] second, and more important, the earth's field sets up the conditions required for the presence of whistler modes, which we would expect to be excited by bomb bursts at *any altitude* and *on either side of the ionosphere*, though the influence of the Van Allen belts on whistlers excited in outer space remains to be evaluated.
4) Finally, we note that because of the large natural background in the frequency range characteristic of whistler propagation—tens to hundreds of kc—we would not expect these signals to be of primary interest in detecting nuclear explosions, but we would expect that they can furnish important secondary information regarding explosions in either the atmosphere or in outer space.

B. A. Lippmann
Lawrence Rad. Lab.
Livermore, Calif.
Consultant, Physics Section
Convair-San Diego
San Diego, Calif.

A Ferromagnetic Amplifier Using Dielectric Loading*

Since Suhl's original paper[1] proposing the ferromagnetic parametric amplifier, a number of experimental amplifiers have been built and tested. Until recently, most of these required rather high pumping powers compared with parametric amplifiers using diodes as variable-reactance elements. Considerable reductions in pumping powers became possible with the use of narrow line-width materials such as single-crystal yttrium iron garnets. Further improvements were reported when use was made of the larger filling factors achievable by operating the amplifier in a modified semistatic mode[2] or in a completely magnetostatic manner.[3]

Preliminary experimental work at Syracuse University[4] indicates that further improvement may be possible by the use of dielectric-loaded cavities. A rectangular cavity of internal dimensions 0.618×0.384 ×0.210 inch was constructed and filled completely (except for the yttrium iron garnet sample) with Stycast Hy K dielectric, of dielectric constant 10. The cavity dimensions were chosen to make the cavity resonant in the TE_{012} mode at the pump frequency of approximately 9300 megacycles per second, and in the TE_{101} mode at the signal frequency of 5900 megacycles per second. (See Fig. 1.) The pump mode was excited from the end wall of a standard X-band guide in the X-Z plane of the cavity. The signal mode was excited by a probe terminating coaxial line in the opposite cavity wall. A disc-shaped sample of 0.132 inch diameter and 0.027 inch thickness was cut from a single crystal of yttrium iron garnet and located at a position of maximum pump and signal fields as shown in Fig. 1.

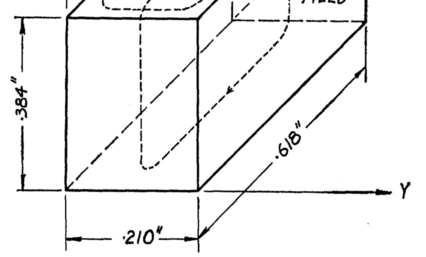

Fig. 1.

* Received by the IRE, July 8, 1960.

[1] H. Suhl, "Theory of the ferromagnetic microwave amplifier," *J. Appl. Phys.*, vol. 28, pp. 1225–1236; November, 1957.

[2] A. D. Berk, L. Kleinman and C. E. Nelson, "Modified semistatic ferrite amplifier," 1958 WESCON CONVENTION RECORD, pt. 3, pp. 9–12.

[3] R. T. Denton, "A ferromagnetic amplifier using longitudinal pumping," PROC. IRE, vol. 48, pp. 937–938; May, 1960.

[4] This work is sponsored by the Rome Air Dev. Center, under Contract No. AF 30(602)-1627.

A dc magnetic field was supplied parallel to the RF signal field at the sample.

Amplification has been observed at dc fields of 700 and 1600 oersteds. The first of these is the field required for resonance of the uniform precessional mode in the sample at the idler frequency, *i.e.*, the difference between pump and signal frequency. The higher field value presumably corresponds to another magnetostatic mode. Pumping powers of a few watts peak were required in the first tests, but theoretical estimates indicate that improvement by at least a factor of ten should be possible. Most of the discrepancy can be ascribed to a poor quality (large line-width) crystal sample.

The uniform precessional mode was identified from observations of the magnetostatic mode spectrum of the disk at the pump frequency. Tests were made with the dc field parallel and normal to the disk. In each case more than 50 resonances were observed as a function of the applied dc field. The uniform precessional mode was most strongly excited in each case. The dc fields required for resonance of the uniform mode in each case, the spread of the spectrum, and the upper and lower bounds of the spectrum were reasonably consistent with the values computed from Kittel's formula and Walker's analysis[5] when use was made of the normally quoted saturation magnetization (1750 oersteds) and gyromagnetic ratio (2.8 megacycles/oersted) of yttrium iron garnet and a demagnetization factor of 0.76 normal to the disk.[6]

Based upon the above preliminary results, it is felt that dielectric loading of the cavity may eventually lead to a practical low-noise ferromagnetic amplifier. The large effective filling factors obtained this way should make it possible to reduce pumping powers to a small fraction of a watt. Furthermore, the small cavity size makes possible the use of small-airgap permanent magnets in the microwave frequency range in which these amplifiers appear to be most useful at present.

HARRY GRUENBERG
Dept. of Elec. Engrg.
Syracuse University
Syracuse, N. Y.

[5] L. R. Walker, "Magnetostatic modes in ferromagnetic resonance," *Phys. Rev.*, vol. 105, pp. 390–399; January, 1957.

[6] J. A. Osborne, "Demagnetizing factors of the general ellipsoid," *Phys. Rev.*, vol. 67, pp. 351–357; June, 1945.

Low Reverse Leakage Gallium-Arsenide Diodes*

Gallium-arsenide diffused diodes have been reported whose operation as high-Q variable capacitors and as computer diodes compared favorably with the best commercially available of germanium and silicon.[1–3] It is the purpose of this note to describe high-speed gallium-arsenide diffused diodes which, because of their reverse leakage currents between 10^{-12} and 5×10^{-11} amperes and rectification ratios above 10^{10}, have replaced vacuum diodes in applications requiring extremely low reverse leakage and/or high rectification ratios.

The current-voltage characteristics of two such devices are plotted to semi-logarithmic scale in Figs. 1 and 2. At 2 volts the rectification ratios for the two diodes are 1.3×10^{10} and 2.5×10^{11}. The forward current in both devices shows an exp $(qv/2kT)$ voltage dependence over a relatively large range of voltage. If this portion of the characteristic is extrapolated to zero volts, a space charge generated saturation current of about 2×10^{-14} amperes is predicted. If one uses the theory of Sah, Noyce, and Shockley[4] and combines this space charge generated saturation current with the diode area and diode zero bias capacitance, one obtains a value for the carrier lifetime $(\tau_{no}\tau_{po})^{1/2}$ of the order of 1×10^{-9} seconds assuming the trap level to be at the Fermi level for intrinsic material, E_i. This lifetime should be compared with the value of τ_{po} of about 6×10^{-9} seconds determined from hole storage measurements on these diodes.[5]

Preliminary measurements have been made on the I-V characteristics of these devices as a function of ambient and temperature in order to try to understand the mechanisms which contribute to the current in the diodes. The lowest reverse currents have been obtained in dry nitrogen or in vacuum. Exposure to dry oxygen increases the reverse current by an order of magnitude, exposure to wet nitrogen increases it by three to four orders of magnitude. The original low reverse currents can be restored by vacuum baking. The reverse characteristic of many of the diodes exhibits the shape shown in Fig. 2. The current at the higher reverse biases ($\sim$7 volts to breakdown voltage) increases relatively slowly (by a factor of 2 for a 60°C temperature rise) with increasing temperature, while at the lower biases the increase is from one to two orders of magnitude for the same temperature rise and is more closely that expected from the increase in the intrinsic carrier concentration n_i. The preliminary ambient and temperature measurements which have been made give promise that further work may lead to even lower reverse currents.

The above devices and others with similar I-V characteristics were fabricated using vertically-pulled single-crystal gallium-arsenide. This material had net impurity densities $N_D-N_A=5\times10^{16}$ to 2×10^{17} cm^{-3}, room temperature mobilities $\mu\approx3000$ to 3800 cm^2 volt^{-1} sec^{-1} and dislocation densities 5000 to 20,000 cm^{-2}. Diodes have been made from this single crystal material with very high yield and excellent reproducibility. The devices were fabricated by diffusing zinc into wafers of (100) oriented n-type starting material to produce a p-type region of depth 3–6 microns. The difference in breakdown voltage between the diodes of Figs. 1 and 2 is due to different diffusion temperatures and hence a shallower gradient in one device than in the other. Both devices were made from the same starting material. After diffusion the wafers were diced and the dice lapped to 3-mils thickness. Ohmic contact to the n-type bulk was made by alloying to a gold-antimony plated kovar stud. Ohmic contact to the p-diffused region was made by alloying a 0.002-inch diameter sphere of 90 per cent Pb and 10 per cent In into this region. Leads were attached and the device was then etched both to form a mesa defining the diode area (HNO_3, HF, HAc; 2:2:3) and to clean up the junction (HAc, H_2O_2;

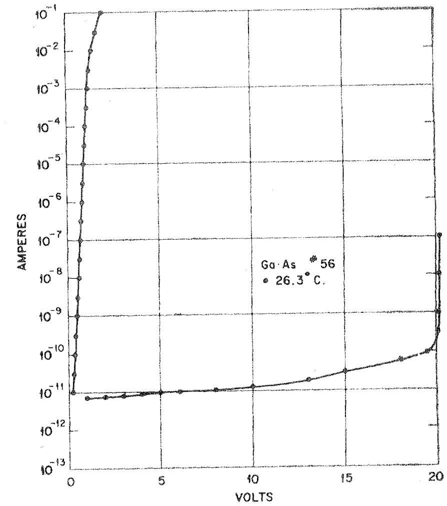

Fig. 1—Current-voltage characteristic (in vacuum) of diode GaAs 56.

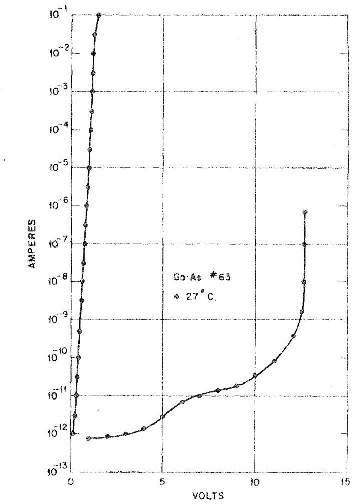

Fig. 2—Current-voltage characteristic (in vacuum) of diode GaAs 63.

* Received by the IRE, July 5, 1960. This work was supported by the U. S. Army, Navy and Air Force.

[1] J. Lowen and R. H. Rediker, "Gallium-arsenide diffused diodes," *J. Electrochem. Soc.*, vol. 107, pp. 26–29; January, 1960.

[2] J. Halpern, J. Lowen and R. H. Rediker, "Gallium-Arsenide Diffused Diodes," presented at the Fifth Annual Electron Devices Conference, Washington, D. C.; October 29–30, 1959.

[3] R. I. Walker, F. A. Cunnell, C. H. Gooch and J. J. Low, "A gallium arsenide switching diode," *J. Electronics Control*, vol. 7, pp. 268–269; September, 1959 (published February, 1960).

[4] C. T. Sah, R. N. Noyce and W. Shockley, "Carrier generation and recombination in p-n junctions and p-n junction characteristics," PROC. IRE, vol. 42, pp. 1228–1243; September, 1957.

[5] R. H. Kingston, "Switching time in junction diodes and junction transistors," PROC. IRE, vol. 42, pp. 829–834; May, 1954.

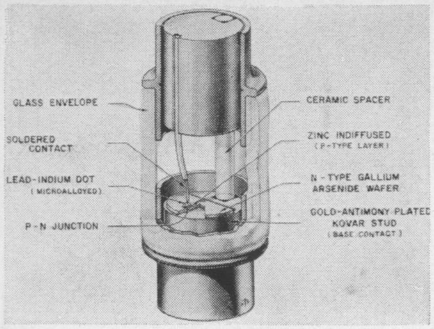

Fig. 3—Artist's representation (not to scale) of a low-leakage gallium-arsenide diode.

3:1). An artist's representation of a completed unit is shown in Fig. 3.

The authors wish to thank T. J. Rey for pointing out important circuit applications of these very low leakage diodes and T. M. Quist for helping in the design of the circuitry to measure the very low currents. They also wish to thank J. Lowen for helpful discussions regarding the fabrication of the devices and especially for developing the etches used, F. M. Sullivan for help in fabricating the diodes, and P. L. Moody for supplying us with the single crystal GaAs.

J. Halpern
R. H. Rediker
Lincoln Lab.
Mass. Inst. Tech.
Lexington, Mass.

Scattering by a Spherical Satellite*

In a recent paper,[1] Vea, Day, and Smith discuss the scattering of electromagnetic waves by a conducting sphere whose radius is large compared to the wavelength. Since the purpose of the paper is to provide information necessary for carrying out imminent propagation experiments, it should be pointed out that the results obtained by these authors are seriously in error. In particular, they deduce a dipole-type scattering pattern for a large sphere, which is at variance with the well-known result that a large, smooth, totally reflecting sphere scatters light by reflection isotropically, while the diffracted light contributes an intense, narrow lobe in the forward direction. The fact that the intensity of the reflected radiation is independent of direction follows easily from geometrical optics, and it can also be derived from the rigorous Mie solution of the electromagnetic problem, as given, for example, by Vea, Day, and Smith's (4) to (6). Indeed, it is the isotropic scattering characteristic of large spheres that makes them such useful standards for monostatic as well as bistatic echo area measurements.

In the paper under discussion, a perfectly conducting sphere of radius a is illuminated by a plane, linearly polarized electromagnetic wave of wavelength λ ($\lambda \ll a$) and maximum electric intensity E_0. The incident wave is traveling in the positive z-direction ($\theta=0$) and is polarized with the electric field parallel to the x-axis ($\phi=0$). This choice of axes corresponds to (1) and (2) of the paper, although Fig. 1 shows the incident wave traveling in the negative z-direction. In terms of bistatic radar cross section, (9) and (17) yield, when a missing factor of r^2 is supplied in the latter equation,

$$\sigma = 4\pi a^2(1 - \sin^2\theta \cos^2\phi).$$

This formula gives a backscattering cross section (echo area) of $4\pi a^2$, which is four times the geometrical cross section and just four times too large. A more serious discrepancy is the completely spurious scattering null which is predicted in the equatorial plane at $\theta=\pi/2$, $\phi=0$ and π.

A correct treatment of the problem of electromagnetic scattering by a perfectly conducting sphere has been given n many places, but an unusually thorough discussion may be found in a recent book by van de Hulst.[2]

In the coordinate system introduced above, the scattered field at a great distance may be written in the form[3]

$$E_\theta = \frac{-iE_0}{kr} e^{i\omega t - ikr} \cos\phi S_2(\theta),$$

$$E_\phi = \frac{iE_0}{kr} e^{i\omega t - ikr} \sin\phi S_1(\theta),$$

where $k=2\pi/\lambda$, and the amplitude functions $S_1(\theta)$ and $S_2(\theta)$ are series of associated Legendre functions with coefficients involving spherical Bessel functions. On the other hand, for a sphere large compared to the wavelength the functions $S_1(\theta)$ and $S_2(\theta)$ may be computed simply by geometrical optics,[4] and turn out to be

$$-S_1(\theta) = S_2(\theta) = \tfrac{1}{2} ika e^{2ika \sin(\theta/2)}.$$

These equations together imply isotropic power scattering by the large sphere, with a scattering cross section

$$\sigma = \pi a^2$$

independent of direction.

It has been shown, both analytically and by numerical computation, that as ka increases the series expressions for $S_1(\theta)$ and $S_2(\theta)$ approach the geometrical optics limit, except of course near the forward scattering direction $\theta=0$, where the Fraunhofer diffraction pattern is superposed on the part of the scattering pattern which is due to reflection. At $\theta=0$ the total scattered field has a large forward lobe, and in the E-plane ($\phi=0$ and π) there is a pronounced dip at an angle which gets closer to $\theta=0$ as a/λ increases. The uniform part of the scattered field can be approximated by geometrical optics, while physical optics will also indicate the dip and the large forward scattering.[5] Numerical summation[6,7] of the Mie series shows these effects developing as the value of ka increases. An extensive bibliography of calculations which have been made using the Mie theory is given by van de Hulst.

The analytical problem of showing that the series for $S_1(\theta)$ and $S_2(\theta)$ approach the geometrical optics limit as $ka \to \infty$ (provided $\theta \neq 0$) was essentially solved by Debye[8] 50 years ago. Vea, Day, and Smith attempted to carry out the limiting process from their (4) and (6), but they appear to have gone astray in replacing the spherical Hankel function $h_n(ka)$ by the first term of its expression in powers of $1/ka$, as given by their (18). This approximation breaks down completely if n and ka are both large and approximately equal, whereas it is well known that important contributions to the sum of the Mie series are made by the terms with $n \approx ka$. Readers interested in the correct analysis will find an account of it in van de Hulst.[9]

As a minor point, we are unable to follow the reasoning in Section C of Vea, Day, and Smith's appendix, where the equivalent gain of the sphere over an isotropic scatterer is said to be computed from the pattern volume. The *volume* of a three-dimensional radiation pattern, where the radius is proportional either to field strength or to power density, has no simple relationship to the total radiated power. If the authors are trying to compute the gain of the dipole-type pattern given by (9), this is well known to be equal to 3/2. In any case, the dipole pattern is irrelevant to the problem at hand.

In summary, the scattering by a conducting spherical satellite which is over 20 wavelengths in diameter can unquestionably be considered isotropic at all aspects of interest for passive satellite reflectors. The calculated variation is less than 1 db for scattering angles greater than 80° if the diameter of the sphere is even as large as $20/\pi$ wavelengths. Furthermore, the choice of polarization will have little effect upon the available scattered power insofar as the satellite reflection properties are concerned.

E. M. Kennaugh
Antenna Lab.
The Ohio State University
Columbus, O.
S. P. Morgan
Bell Telephone Labs., Inc.
Murray Hill, N. J.
H. Weil
Radiation Lab.
Electrical Engineering Dept.
University of Michigan
Ann Arbor, Mich.

* Received by the IRE, May 26, 1960.

[1] T. H. Vea, J. B. Day, and R. T. Smith, "The use of a passive spherical satellite for communication and propagation experiments," Proc. IRE, vol. 48, pp. 620–624; April, 1960.

[2] H. C. van de Hulst, "Light Scattering by Small Particles," John Wiley and Sons, Inc., New York, N. Y.; 1957.

[3] Van de Hulst, *op. cit.*, pp. 124–125.

[4] Van de Hulst, *op. cit.*, p. 223.

[5] K. M. Siegel, H. A. Alperin, R. R. Bonkowski, J. W. Crispin, A. L. Moffett, C. E. Schensted, and I. V. Schensted, "Bistatic radar cross sections of surfaces of revolution," *J. Appl. Phys.*, vol. 26, pp. 297–305; March, 1955.

[6] Van de Hulst, *op. cit.*, p. 163.

[7] R. W. P. King and T. T. Wu, "The Scattering and Diffraction of Waves," Harvard University Press, Cambridge, Mass., pp. 205–213; 1959.

[8] P. Debye, "Der Lichtdruck auf Kugeln von beliebigem Material," *Ann. Phys.*, Ser. 4, vol. 30, pp. 57–136; August, 1909.

[9] Van de Hulst, *op. cit.*, pp. 208–214.

Scattering Properties of Large Spheres*

If the plane wave $\boldsymbol{E}_i = E_0\hat{x}\exp[i(kz+\omega t)]$ illuminates a perfectly conducting sphere of radius a, the secondary field at a large distance from the sphere is, according to geometrical optics, given by

$$\boldsymbol{E}_s \underset{r\to\infty}{\longrightarrow} (-\cos\phi\hat{\theta} + \sin\phi\hat{\phi})\frac{a}{2r} \cdot \exp\left[i\left(2ka\cos\frac{\theta}{2} - kr + \omega t\right)\right].$$

In a recent paper, Vea, Day, and Smith[1] have started from the exact solution

$$\boldsymbol{E}_s = \frac{1}{ik}\sum_{n=1}^{\infty}\frac{2n+1}{n(n+1)}i^n\left[\frac{\psi_n'(ka)}{\xi_n^{(2)\prime}(ka)}\cdot \text{curl curl}\left[rh_n^{(2)}(kr)P_n^1(\cos\theta)\cos\phi\right] + \frac{\psi_n(ka)}{\xi_n^{(2)}(ka)}\text{curl}\left[rh_n^{(2)}(kr)P_n^1(\cos\theta)\cos\phi\right]\right]$$

$$\psi_n(x) = xj_n(x) = \sqrt{\frac{\pi x}{2}}J_{n+1/2}(x),$$

$$\xi_n^{(2)}(x) = xh_n^{(2)}(x) = \sqrt{\frac{\pi x}{2}}H_{n+1/2}^{(2)}(x)$$

and have arrived at the erroneous result

$$\boldsymbol{E}_s \underset{r\to\infty}{\longrightarrow} (-\cos\theta\cos\phi\hat{\theta} + \sin\phi\hat{\phi})\frac{a}{r} \cdot \exp\left[i(ka\cos\theta + ka - kr + \omega t)\right].$$

These authors have erred in using the asymptotic estimate

$$\xi_n^{(2)}(x) \sim i\exp\left[-ix + in\frac{\pi}{2}\right], \qquad x = ka$$

for all values of n, although it is actually valid only for $n \ll ka$. The objections to the use of this estimate for all values of n has a long history.

Rayleigh[2] discussed its use in his 1872 paper on diffraction of sound by a sphere. In 1903, MacDonald[3] made this error in a study of diffraction of radio waves around a sphere and was immediately criticized by both Rayleigh[4] and Poincaré.[5] MacDonald[6] conceded his mistake, and for several years the mathematical physicists were unable to show that the exact solutions for the diffraction of waves by spheres and cylinders are consistent with geometrical optics when the radius greatly exceeds the wavelength. In 1908, Debye[7] showed how to obtain an asymptotic estimate to the exact solution of the cylinder problem which is identical with the result predicted by geometrical optics. The exact solution for the sphere problem has been shown to lead to the optics result by Nicholson,[8,9] Bromwich,[10] and White.[11]

In a report which is now in preparation,[12] we will show that the estimates obtained from geometrical optics are the leading terms in asymptotic expansions of the form

$$\hat{\theta}\cdot\boldsymbol{E}_s \underset{\substack{r\to\infty\\ ka\to\infty}}{\longrightarrow} -\cos\phi\frac{a}{2r}\exp\left[i\left(2ka\cos\frac{\theta}{2} - kr + \omega t\right)\right]\left[1 + i\frac{1}{2(ka)\cos^3\frac{\theta}{2}} - \frac{7\sin^2\frac{\theta}{2}}{4(ka)^2\cos^6\frac{\theta}{2}} - i\frac{79\sin^2\frac{\theta}{2} + 33\sin^4\frac{\theta}{2}}{8(ka)^3\cos^9\frac{\theta}{2}} + \frac{8 + 1076\sin^2\frac{\theta}{2} + 1401\sin^4\frac{\theta}{2} + 210\sin^6\frac{\theta}{2}}{16(ka)^4\cos^{12}\frac{\theta}{2}} + \cdots\right]$$

$$\hat{\phi}\cdot\boldsymbol{E}_s \underset{\substack{r\to\infty\\ ka\to\infty}}{\longrightarrow} \sin\phi\frac{a}{2r}\exp\left[i\left(2ka\cos\frac{\theta}{2} - kr + \omega t\right)\right]\left[1 + i\frac{1 - 2\sin^2\frac{\theta}{2}}{2(ka)\cos^3\frac{\theta}{2}} + \frac{7\sin^2\frac{\theta}{2} - 2\sin^4\frac{\theta}{2}}{4(ka)^2\cos^6\frac{\theta}{2}} + i\frac{63\sin^2\frac{\theta}{2} + 7\sin^4\frac{\theta}{2}}{8(ka)^3\cos^9\frac{\theta}{2}} + \frac{8 - 836\sin^2\frac{\theta}{2} - 683\sin^4\frac{\theta}{2} - 84\sin^6\frac{\theta}{2}}{16(ka)^4\cos^{12}\frac{\theta}{2}} + \cdots\right].$$

Care must be exercised in using these asymptotic expansions because they describe only the wave *reflected* from the sphere. The wave *diffracted* around the sphere (sometimes called a creeping wave) is generally important if

$$\left(\frac{ka}{2}\right)^{1/3}(\pi - \theta) < 8.$$

It is a curious fact that the introduction of the improper asymptotic estimate for $\zeta_n^{(2)}(ka)$ when studying *large perfectly conducting* spheres leads to patterns for the scattered energy which are identical with the Rayleigh scattering patterns for *small dielectric* spheres. If m denotes the index of refraction, the Rayleigh scattering law is

$$\boldsymbol{E}_s \underset{\substack{r\to\infty\\ ka\ll 1}}{\longrightarrow} -(-\cos\theta\cos\phi\hat{\theta} + \sin\phi\hat{\phi}) \cdot \frac{a}{r}\left[(ka)^2\frac{m^2-1}{m^2+2}\right]\exp\left[i(-kr+\omega t)\right].$$

The corresponding result for Rayleigh scattering by small conducting spheres is

$$\hat{\theta}\cdot\boldsymbol{E}_s \underset{\substack{r\to\infty\\ ka\ll 1}}{\longrightarrow} \frac{a}{r}(ka)^2\left[\cos\theta + \tfrac{1}{2}\right]\cos\phi \cdot \exp\left[-ikr + i\omega t\right]$$

$$\hat{\phi}\cdot\boldsymbol{E}_s \underset{\substack{r\to\infty\\ ka\ll 1}}{\longrightarrow} -\frac{a}{r}(ka)^2\left[\frac{\cos\theta}{2} + 1\right]\sin\phi \cdot \exp\left[-ikr + i\omega t\right]$$

and therefore cannot be obtained from the dielectric result by merely letting m tend to infinity.

In view of the above remarks, we must conclude that the results of Vea, Day, and Smith do not describe the reflection properties of large conducting spheres and no useful results are contained in their article.

N. A. Logan
Lockheed Missiles and Space Div.
Sunnyvale, Calif.

* Received by the IRE, June 21, 1960.

[1] T. H. Vea, J. B. Day, and R. T. Smith, "The use of a passive spherical satellite for communication and propagation experiments," Proc. IRE, vol. 48, pp. 620–624; April, 1960.

[2] Lord Rayleigh, "Investigation of the disturbance produced by a spherical obstacle on the waves of sound," *Proc. London Math. Soc.*, vol. 4, pp. 253–283; 1872.

[3] H. M. Macdonald, "The bending of electric waves round a spherical obstacle," *Proc. Roy. Soc. (London) A*, vol. 71, pp. 251–258; 1903.

[4] Lord Rayleigh, "On the bending of waves round a spherical obstacle," *Proc. Roy. Soc. (London) A*, vol. 72, pp. 40–41; 1903. ("Scientific Papers," Cambridge University Press, New York, N. Y., vol. 5, pp. 112–114; 1912.)

[5] H. Poincaré, "Upon the diffraction of electric waves; upon a paper of Macdonald," *Proc. Roy. Soc. (London) A*, vol. 72, pp. 42–52; 1903.

[6] H. M. Macdonald, "The bending of electric waves round a conducting obstacle: amended result," *Proc. Roy. Soc. (London) A*, vol. 72, pp. 59–68; 1903.

[7] P. Debye, "The electromagnetic field surrounding a cylinder, and the theory of the rainbow," *Physik Z.*, vol. 9, pp. 775–778; 1908.

[8] J. W. Nicholson, "The scattering of light by a large conducting sphere," *Proc. London Math. Soc.*, vol. 9, pp. 67–80; 1910.

[9] J. W. Nicholson, "The scattering of light by a large conducting sphere (second paper)," *Proc. London Math. Soc.*, vol. 11, pp. 277–284; 1912.

[10] T. Bromwich, "The scattering of plane electric waves by spheres," *Phil. Trans. Roy. Soc. (London) A*, vol. 220, pp. 189–206; 1920.

[11] F. P. White, "The diffraction of plane electromagnetic waves by a perfectly reflecting sphere," *Proc. Roy. Soc. (London) A*, vol. 100, pp. 505–525; 1922.

[12] N. A. Logan, "General Research in Diffraction Theory III. Asymptotic Expansions of Exact Solutions for Diffraction by Cylinders and Spheres," Lockheed Missile Systems Div., Sunnyvale, Calif., Tech. Rept. No. LMSD 288089, in preparation.

WWV and WWVH Standard Frequency and Time Transmissions*

The frequencies of the National Bureau of Standards radio stations WWV and WWVH are kept in agreement with respect to each other and have been maintained as constant as possible with respect to an improved United States Frequency Standard (USFS) since December 1, 1957.

The nominal broadcast frequencies should, for the purpose of highly accurate scientific measurements, or of establishing high uniformity among frequencies, or for removing unavoidable variations in the broadcast frequencies, be corrected to the value of the USFS, as indicated in the table below.

The characteristics of the USFS, and its relation to time scales such as ET and UT2, have been described in a previous issue,[1] to which the reader is referred for a complete discussion.

* Received by the IRE, August 29, 1960.

[1] Refer to "United States National Standards of Time and Frequency," Proc. IRE, vol. 48, pp. 105–106; January, 1960.

The WWV and WWVH time signals are also kept in agreement with each other. Also they are locked to the nominal frequency of the transmissions and consequently may depart continuously from UT2. Corrections are determined and published by the U. S. Naval Observatory. The broadcast signals are maintained in close agreement with UT2 by properly offsetting the broadcast frequency from the USFS at the beginning of each year when necessary. This new system was commenced on January 1, 1960. The last time adjustment was a retardation adjustment of 0.02 *s* on December 16, 1959.

WWV Frequency
With Respect to U. S. Frequency Standard

1960 July 1600 UT	Parts in 10^{10}†
1	−147
2	−148
3	−148
4	−148
5	−148
6	−148
7	−149
8	−149
9	−149
10	−149
11	−149
12	−149
13	−149
14	−149
15	−149
16	−149
17	−149
18	−149
19	−149
20	−149
21	−149
22	−148
23	−148
24	−148
25	−148
26	−147
27	−147
28	−147
29	−147
30	−147
31	−147

† A minus sign indicates that the broadcast frequency was low.

National Bureau of Standards
Boulder, Colo.

Correction to "Direct Reading Noise Figure Measuring Device"*

George Bruck, author of the above, which appeared on page 1342 of the July, 1960, issue of Proceedings, has been advised of the following by W. W. Mumford of Bell Telephone Laboratories, Whippany, N. J.

In the third column, second to the last paragraph, the formula for the noise figure appears. The text following this formula should read "where F_0 is the excess noise ratio of the noise source. . . ."

The excess noise ratio of the noise source is the ratio of the excess power of the noise source to the thermal power at 290° K.

* Received by the IRE, August 12, 1960.

Correction to "Absolutely Stable Hybrid Coupled Tunnel Diode Amplifier"*

John J. Sie, author of the above Correspondence, which appeared on page 1321 of the July, 1960 issue of Proceedings, has advised the Editor of the following.

Eq. (2) should read:

$$|S_{21}|^2 = \frac{\left(1 + \frac{G}{G_0} - \frac{G_1}{G_0}\right)^2 + B^2}{\left(1 - \frac{G}{G_0} + \frac{G_1}{G_0}\right)^2 + B^2}.$$

In (3),

$$F = 1 + \frac{G_1 + 20I_0}{G_0}\eta + \frac{|S_{22}|^2}{|S_{21}|^2}$$

and

$$\eta = \frac{4}{\left(1 + \frac{G}{G_0} - \frac{G_1}{G_0}\right)^2 + B^2}$$

where B is the normalized susceptance of the shunt circuit.

* Received by the IRE, July 25, 1960.

Some Results on Diode Parametric Amplifiers*

Parametric amplifiers at S and X band have been studied at room temperature with the following results:

S Band

$f_s = 3$ kmc
$f_p = 11.9$ kmc
Gain = 17 db
Bandwidth = 50 mc
Noise Figure = 1.6 db ± 0.2 db
Diode MA450F-R $f_c = 80$ kmc
Pump Power = 10 mw
Calculated NF = 1.74 db,

X Band

$f_s =$ 9900 mc
$f_p =$ 19,800 mc
Gain = 20 db
Bandwidth = 25 mc
Noise Figure = 1.2 db ± 0.5 db Double Sideband
Diode MA450H-Rf_c = 100 kmc
Radar Noise Figure = 4.2 db ± 0.5 db
Pump Power = 120 mw
Calculated NF = 1.2 db

The relationship of Penfield[1] was used to check theoretically these results for single sideband operation. The noise figure is

$$F = 1 + \frac{\omega_s}{\omega_i}\left[\frac{m^2\omega_c^2 + \gamma\omega_i^2}{m^2\omega_c^2 - \omega_i\omega_s}\right],$$

where

ω_c = Cutoff frequency of the diode based on C_{min}
ω_i = Idler frequency
m = Modulation ratio = $|S_1|/S_{max}$
$|S_1|$ = Pump frequency component of elastance
S_{max} = Maximum varactor elastance
$\gamma = (R_i + R_s)/R_s$
R_s = Varactor series resistance
R_i = Real part of the external idler terminating impedance.

For the case under consideration,

$m = 0.2$
$\gamma = 1.$

I. Goldstein
J. Zorzy
Raytheon Co.
Missile System Div.
Bedford, Mass.

* Received by the IRE, April 18, 1960.
[1] P. Penfield, Jr., private communication.

Some Parametric Amplifier Circuit Configurations and Results*

The application of two techniques, well known to the microwave engineer, have been applied to parametric amplifiers. These are quarter-wave-coupled filter techniques and the cascading of the amplifiers. First, a simple circuit configuration for the parametric amplifier was selected and this was a Hewlett-Packard 440A crystal mount which makes a good degenerate amplifier at S band. I call the filter type an active quarter-wave-coupled filter as compared to a passive one. A schematic of the circuit is shown in Fig. 1. The cold characteristic of this circuit is shown in Fig. 2.

The active characteristic is shown in Fig. 3.

In the reverse direction the gain characteristic is shown in Fig. 4.

The reverse characteristics actually indicated gain off frequency for given settings of the amplifier tuning stubs. The results are summarized in Table I.

This amplifier with adjustment was also operated in a nondegenerate mode with the following characteristics:

Gain = 10 db,
BW = 17 db,
$f_s = 2600$ mc,
$f_p = 10{,}800$ mc,
Pump power = 500 mw.

In the backward wave mode of operation, a very narrow band-pass of 1 mc at a gain of 10 db was observed which was tunable over a 15-mc band by varying pump frequency and amplitude. The signal and pump frequencies were the same as in the forward wave mode.

* Received by the IRE, April 15, 1960.

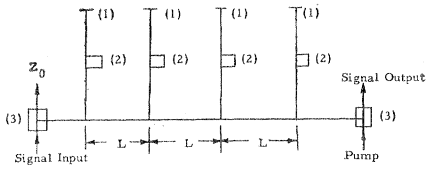

Fig. 1—1) Tuning stub; 2) Varactor; 3) Diplexer; $l=0.5$ λ signal; $L=0.7$ λ signal.

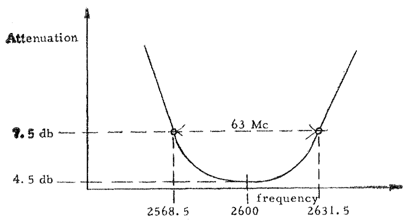

Fig. 2.

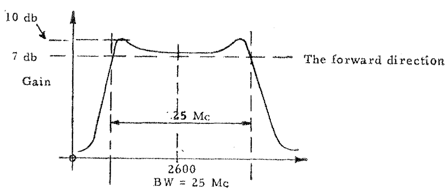

Fig. 3.

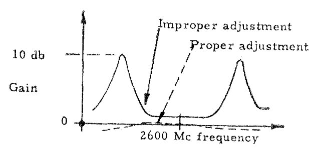

Fig. 4.

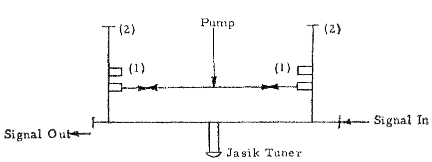

Fig. 5—1) Diode; 2) Tuning stub.

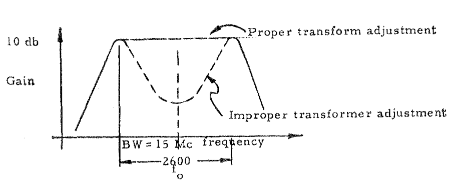

Fig. 6.

TABLE I

Pump	Direction	Gain	Bandwidth
On	Input to Output	10 db	25 mc
On	Output to Imput	0 to −1.5 db	25 mc
Off	Input to Output	4.5 db	63 mc

$f_s=2600$ mc.
$f_p=5200$ mc.
Pump power = 100 mw.
NF = 5 db, double-sideband.

CASCADING RESULTS

The basic circuit used in this experiment is shown in Fig. 5. With adjustment of the amplifiers and Jasik tuner, the following data were obtained:

Gain = 10 db,
BW = 15 mc,
$f_p=5200$,
$f_s=2600$,
Pump power = 6 mw.

The coupling between the ampliqer circuits is shown in Fig. 6.

In summary, two techniques have been experimentally demonstrated to show that increased gain bandwidth can be obgained.

I. GOLDSTEIN
Raytheon Co.
Missile Systems Div.
Bedford, Mass.

Gain Inconsistencies in Low-Frequency Reactance Parametric Up-Converters*

One of the problems that plagues the designer of low-frequency up-converter reactance parametric amplifiers is the fact that the gain of the amplifier is seldom equal to the expected value calculated from the ratio of the upper sideband frequency to the signal frequency.

It is the purpose of this note to offer a first-order explanation of this phenomenon and suggest ways to improve the performance of these amplifiers.

Assume that a lossless parametric diode may be represented, in *ABCD* matrix form, by the equivalent circuit as shown in Fig. 1.

E_s, I_s are signal frequency components at ω_s;

E_m, I_m are upper sideband components at ω_m;

$$|A| = \sqrt{\frac{\omega_s}{\omega_m}\frac{C_p^*}{C_p}} \cdot \begin{vmatrix} 0 & i\dfrac{1}{|C_p|\sqrt{\omega_m\omega_s}} \\ j|C_p|\sqrt{\omega_m\omega_s} & 0 \end{vmatrix};$$

$C_p=C_1v_p$, where C_1 is the nonlinear term in the diode capacitance expansion; $C=C_0+C_1v$, and $v_p=V_pe^{j\theta p}$ is the pump voltage.

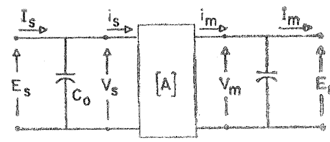

Fig. 1.

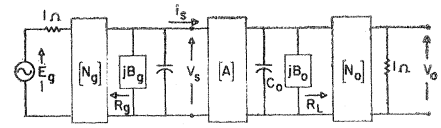

Fig. 2.

Let the amplifier have the form as shown in Fig. 2. $[N_g]$ and $[N_0]$ are coupling networks matching the amplifier to the source and load. $[N_g]$ and $[N_0]$ may be represented as

$$[N_g] = \begin{vmatrix} 1/\sqrt{R_g} & 0 \\ 0 & \sqrt{R_g} \end{vmatrix}$$

and

$$[N_0] = \begin{vmatrix} \sqrt{R_L} & \\ 0 & 1/\sqrt{R_L} \end{vmatrix}$$

where R_g and R_L are the transformed source and load impedances. We will assume single frequency operation such that the capacitances C_0 at the input and output are tuned out by the susceptances jB_g and jB_0.

The transfer matrix for the amplifier can be written as

$$[T] = [N_g][A][N_0] = \begin{vmatrix} T_{11} & T_{12} \\ T_{21} & T_{22} \end{vmatrix}$$
$$= \sqrt{\frac{\omega_s}{\omega_m}\frac{C_p^*}{C_p}} \begin{vmatrix} 0 & j\dfrac{1}{\sqrt{\omega_s\omega_m}\,|C_p|\,\sqrt{R_LR_g}} \\ j\sqrt{\omega_m\omega_s}\,|C_p|\,\sqrt{R_LR_g} & 0 \end{vmatrix}. \qquad (1)$$

Assuming that $R_g=R_L=R$,

$$[T] = \sqrt{\frac{\omega_s}{\omega_{mn}}\frac{C_p^*}{C_p}} \cdot \begin{vmatrix} 0 & j\dfrac{1}{{}_n\sqrt{\omega_s\omega_m}\,|C_p|\,R} \\ j\sqrt{\omega_m\omega_s}\,|C_p|\,R_n & 0 \end{vmatrix}. \qquad (2)$$

The power gain may be expressed[1] as

$$G_p = \frac{P_m}{P_n} = \frac{4\left(\dfrac{\omega_m}{\omega_s}\right)}{\left|\sum_{ij} T_{ij}\right|^2}. \qquad (3)$$

Thus

$$G_p = \frac{4\dfrac{\omega_m}{\omega_s}}{2 + \omega_m\omega_sR^2|C_p|^2 + \dfrac{1}{\omega_m\omega_sR^2|C_p|^2}}. \qquad (4)$$

* Received by the IRE, April 4, 1960.

[1] H. Seidel and G. Hermann, "Circuit aspects of parametric amplifiers," 1959 IRE WESCON CONVENTION RECORD, pt. 2, pp. 83–90.

It is seen from (4) that

$$G_p = G_{p\,\max} = \frac{\omega_m}{\omega_s}$$

only when

$$\omega_m \omega_s R^2 |C_p|^2 = 1.$$

The input admittance at the v_s, i_s terminals with C_0 tuned out at the output is found from

$$\begin{vmatrix} v_s \\ i_s \end{vmatrix} = \sqrt{\frac{\omega_s}{\omega_m}\frac{C_p{}^*}{C_p}} \cdot \begin{vmatrix} 0 & j\dfrac{1}{\sqrt{\omega\,\omega_m}\,|C_1|\,R} \\ j\sqrt{\omega_s\omega_m}\,|C_p|\,R_n & 0 \end{vmatrix} \cdot \begin{vmatrix} \sqrt{R_L} & 0 \\ 0 & \dfrac{1}{\sqrt{R_L}} \end{vmatrix} \begin{vmatrix} 1 & 0 \\ 1 & 1 \end{vmatrix} \begin{vmatrix} v_0 \\ 0 \end{vmatrix} \tag{5}$$

to be

$$y_s = \frac{i_s}{v} = \frac{\omega_m \omega_s R^2 |C_p|^2}{R}. \tag{6}$$

Again, it is noticed that when

$$\omega_m \omega_s R^2 |C_p|^2 = 1,$$

$$y_s = 1/R$$

which is the condition for match at the input.

It is therefore evident that the term $\omega_m \omega_s R^2 |C_p|^2$ is of major importance in the operation of the amplifier.

At lower frequencies it is not always possible to make this term unity.

As an example, an experimental amplifier in our laboratory has the following operating parameters:

$$F_s = 220 \text{ mc},$$
$$F_p = 1120 \text{ mc},$$
$$F_m = 1340 \text{ mc},$$
$$R_g = R_L = R = 50 \text{ ohms}.$$

The expected value of gain $G_{p\max} = 1340/220 = 6.1$.

To achieve $\omega_m \omega_s R^2 |C_p|^2 = 1$ would require that $|C_p| = 5.84$ $\mu\mu$f.

An input admittance measurement yielded a measured value of $|C_p| = 1.85$ $\mu\mu$f giving $\omega_m \omega_s R^2 |C_p|^2 = 0.1$. The calculated value of the gain was then 2.02. The measured gain was 1.97, which is in very close agreement with the calculated value. Other diodes were tested and again very close agreement was found.

Three possible remedies are suggested:

1) Obtain diodes with the proper value of $|C_p|$ to make $\omega_m \omega_s R^2 |C_p|^2 = 1$.
2) Design amplifiers using that value of R necessary to make $\omega_m \omega_s R^2 |C_p|^2 = 1$.
3) Operate at a pump-to-signal frequency ratio that makes $\omega_m \omega_s R^2 |C_p|^2 = 1$.

That is,

$$\omega_s(\omega_p + \omega_s) R^2 |C_p|^2 = 1$$

or

$$\left.\frac{\omega_p}{\omega_s}\right|_{\text{opt}} = \left[\frac{1}{(R|C_p|\,\omega_s)^2} - 1\right].$$

This pump-to-signal frequency ratio is not always practical, as in the case of our experimental amplifier where

$$\left.\frac{\omega_p}{\omega_s}\right|_{\text{opt}} = 60.3.$$

It is hoped that the above discussion may be of some help to the designers of low-frequency parametric up-converters. The authors wish to acknowledge gratefully the help of M. Subramanian who did the experiments necessary to verify these results. We also wish to thank the Magnavox Company for their support in this work.

A. K. Kamal
A. J. Holub
Millimeter Wave Res. Lab.
Dept. of Elec. Engrg.
Purdue University
Lafayette, Ind.

Parametric Amplification Properties in Transistors*

A new mode of operation for high-frequency transistors with special input characteristics has been discovered, whereby useful conversion gain can be obtained beyond the normal frequency cutoff of the unit. Transistor development has made it clear[1] that shrinking the geometry in transistors to reduce the junction capacitances helps to improve the performance at high frequencies at the sacrifice of power handling capabilities. The parametric amplifier-transistor can be made with larger dimensions for a given frequency of operation than a conventional high-frequency transistor and, therefore, has a much higher power handling capability.

Commercially available high-frequency transistors offer a maximum frequency of oscillation around 1 kmc (2N700, 2N502). These can yield a power gain of about 6.2 db at 450 mc. In the new mode of operation, Hughes experimental germanium transistors (GXG4 Model II) measured 72 db conversion gain (from input to IF) at 450 mc with a signal-to-noise ratio of 21 db at a bandwidth of approximately 20 kc and at an input signal level of 1 μv. The maximum frequency of oscillation for these units was 600 mc. Other measurements have shown a gain of 50 db at a bandwidth of 750 kc. In an up-conversion mode, gain can be produced at harmonics of the fundamental frequency of oscillation. The emitter cutoff frequency of 2.4 kmc at a zero bias capacitance of 2 $\mu\mu$f limited the operation at harmonics above these values. The transistors are with reason, therefore, called "parametric-amplifying" or "variable reactance" devices.

The new circuit, in which the reported performance data were taken, is given in Fig. 1. A novel oscillator with an autotransformer serves as the "pump" oscillator and its frequency is determined by a high Q tank circuit $L_L C_L$ with a butterfly arrangement. A negative resistance arises from a capacitive reactance which is reflected through the autotransformer from the output back into the input under oscillatory conditions. An additional deviation from the regular oscillator circuit is an inductance L_S placed in the input loop, which will react with the negative resistance. The amount of feedback, which also determines the negative resistance, can be adjusted by aid of the feedback capacitance C_F. The variable reactance properties necessary for parametric amplification performance are especially designed into Hughes experimental germanium mesa transistors (GXG4 Model II) and are sometimes present in commercially existing high-frequency transistors, *e.g.* Mesa 2N700, MADT 2N502.

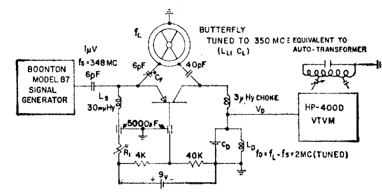

Fig. 1—Circuit arrangement for the variable reactance transistor oscillator-amplifier circuit. Conversion gain is measured at a frequency of 2 mc.

The complex input impedance measurement establishes the variable reactance characteristics inherent to these transistors. For a Hughes GXG4 transistor, the complex input impedance h_{ib} is given as a function of frequency for two emitter current levels in Figs. 2(a) and 2(b). This measurement offers a possible method of obtaining frequency cutoff characteristics of transistors, since the α-current generator, which is also complex, is implicitly contained in h_{ib}. In our work the α-current generator has been replaced by the relation

$$\alpha = \frac{\alpha_0 \exp(-jmf/fc)}{1 + j(f/fc)}$$

where

α_0 = low-frequency α transistor,
f = frequency variable,
f_c = frequency cutoff of transistor,
m = a constant of the phase vector, which is 0.21 for a diffusion transistor, but greater than 0.21 for drift transistors. (The Hughes GXG4 unit has $m = 0.6$.)

The complex plot of current gain (α) is reflected in the curves for the complex h_{ib} behavior, Fig. 2. The point of interest in Fig. 2(a) is at the frequency $f = 350$ mc where h_{ib} is imaginary and equal to $-j25$ ohms, and in Fig. 2(b) is equal to $+j36$ ohms at the same frequency. The difference in the two representations is that the two values are taken at the same frequency, but at different current levels, and it is obvious that the input impedance must pass the real axis within that particular current interval. Graphically, Fig. 3 illustrates the impedance vs emitter current relation and reveals a variable reactance around the point where

* Received by the IRE, May 2, 1960.

[1] R. E. Davis, C. H. Bittman, and R. J. Gnaedinger, "Microwave Germanium Transistors," presented at the Fifth Annual Electron Devices Conference, Washington, D. C.; October 29–30, 1959.

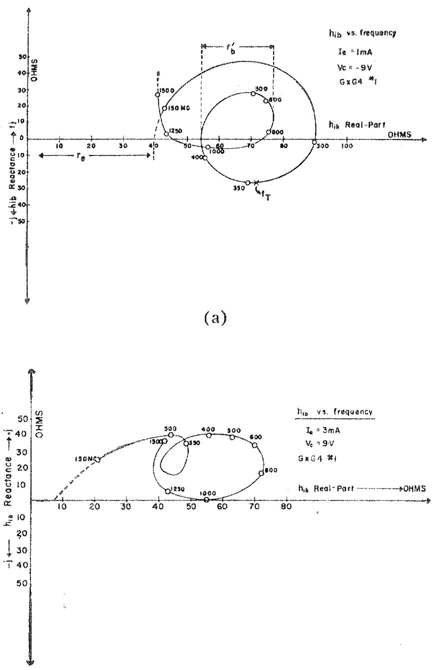

Fig. 2—(a) Complex input impedance h_{ib} measurement with frequency as variable for a Hughes GXG4 transistor. Bias condition: emitter current I_e=1 ma, collector voltage $V_c=-9$ v.(b) Complex input impedance h_{ib} measurement as for (a) but at I_e=3 ma.

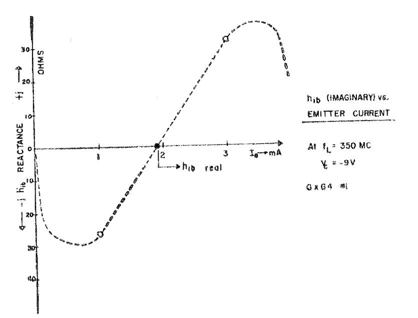

Fig. 3—Plot of imaginary part of the input impedance h_{ib} vs emitter current at a fixed frequency, *e.g.* 350 mc.

the current is 2 ma. Furthermore, it is conclusive that, for a particular frequency, the input impedance of a certain transistor can be made real for a specific current. Accomplishing this is referred to as current tuning. Considering the dc bias arrangement in Fig. 1, the current tuning for a fixed oscillating frequency f_L can be performed by adjusting R_1. The effectiveness of this procedure can be seen in Fig. 4(a), where *conversion* gain is plotted as a function of emitter current. To meet the condition of tuning requires continuation of oscillation. This is not easily met in all existing high-frequency transistors, but can be designed into the device. The amount of feedback can be adjusted at will and one can obtain stable gains for desirable settings by avoiding disturbance of current tuning, and matching conditions for L_S.

The excellent gain performance is due not only to variable reactance behavior of the input impedance, but also to the feed-

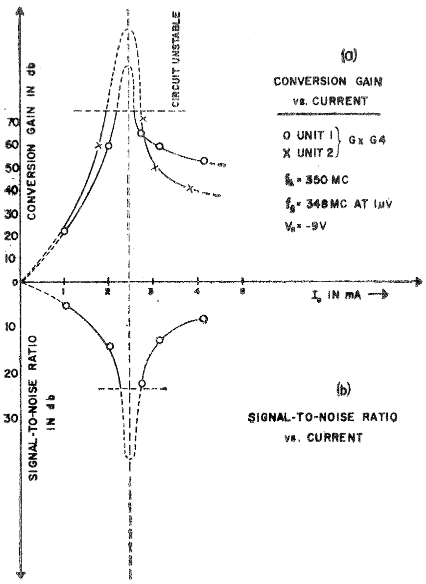

Fig. 4—(a) Conversion gain, measured in circuit of Fig. 1 for a GXG4 transistor vs emitter current at collector voltage of $V_c=-9$ v. (b) Signal-to-noise ratio of the same transistor under the test conditions of a versus current at a bandwidth of approximately 20 kc.

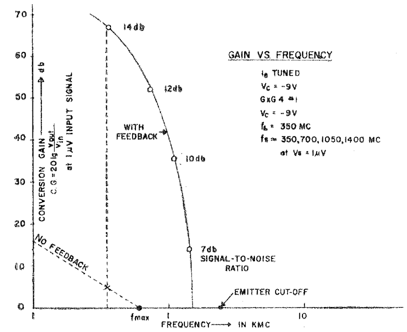

Fig. 5—Conversion gain vs frequency with and without feedback, including signal frequencies in multiples of the oscillator frequency, *e.g.* harmonics.

back amplifier properties[2] of the circuit, even under oscillatory conditions. These advantages are evidenced from results presented in Figs. 4(a), 4(b) and Fig. 5 and they are

1) increase in frequency gain bandwidth,
2) noise reduction,
3) reduction in the influence of transistor parameter variations upon gain, which increases stability since now external circuitry elements determine the performance.

The coordination of circuit development and device design produced maximum conversion gains of the fundamental frequency of operation of 90 db with a signal-to-noise ratio of 30 db. The best performance at harmonics of the fundamental oscillation frequency occurred at 1.4 kmc with 14 db conversion gain and a signal-to-noise ratio of 7 db at a bandwidth of 150 kc. The true noise performance during this measurement reveals a noise figure of 2–3 db above ambient. The measurements at multiples of the fundamental oscillation frequency are given in Fig. 5. From the maximum frequency of oscillation for that particular transistor, only 5 db gain can be predicted at 350 mc. With feedback operation and current tuning in the new mode, the conversion gain was 66 db. Without feedback we assumed the 6 db per octave slope. The slope or falloff of gain with applied feedback vs frequency is not understood at the present writing and extrapolations of the measurements to produce ultimate performances are subject to speculation. However, it is reasonable to believe that the emitter cutoff frequency alone in present devices will limit the performance to frequencies of the order of approximately 2.4 kmc. In regard to performance it may be said that under present circumstances the matching conditions in the test circuits are not perfected and proper transistor designs are not fully explored so that the possibilities of extending the useful frequency range in transistors into the microwave region of 5–10 kmc is most likely in the near future.

Although the theoretical development is not yet completed, enough quantitative experimental evidence has been presented to manifest the existence of a *parametric-amplifier transistor*. The up-conversion mode of operation has been verified experimentally and a detailed analysis of the nonlinear elements which produce the conversion gain has been initiated in regard to harmonic power generation. The results will be published as soon as the work is completed.

The authors are indebted to both managements and are especially grateful to Dr. R. A. Gudmundsen and G. M. Lebedeff for their valuable time devoted to discussions on this matter.

R. Zuleeg
Hughes Aircraft Co.
Semiconductor Div.
Newport Beach, Calif.
V. W. Vodicka
Lenkurt Electric Company, Inc.
General Telephone and
Electronics Corp
San Carlos, Calif

[2] R. I. Shea, "Principles of Transistor Circuits," John Wiley and Sons, Inc., New York, N. Y.; 1953.

The Electron Content and Distribution in the Ionosphere*

In a recent letter,[1] results were given of electron content measurements determined from the Faraday rotation rate of transmissions from the satellite 1958δ_2. From this data and estimates of the electron content below the maximum of the F_2 layer, the ratio of the number of electrons above the F_2 maximum to that below was estimated.

* Received by the IRE, April 22, 1960.

[1] T. G. Hame and W. D. Stuart, "The electron content and distribution in the ionosphere," Proc. IRE, vol. 48, pp. 364; March, 1960.

More exact data[2] have since been received concerning the electron content below the F_2 maximum and indicates that the estimated nighttime value of the electron distribution ratio was too low. Fig. 1 shows the electron content to the satellite height, the electron content below the F_2 maximum and the electron distribution ratio during the pre-dawn period for May 4–11, 1959. The distribution ratio is between 3.1 and 4.7, which is consistent with the results given by Bauer, Daniels[3] and Evans.[4,5] The electron distribution ratio during the daytime has also been determined for the period March 4 to April 20, 1959. Excluding measurements during periods of high geomagnetic activity, a mean value of 2.3 was obtained.

To illustrate the variations in observed electron content measurements, the electron content is plotted in Fig. 2(a) as a function of increasing date and local time for the period March 21 to April 13, 1959. If this data is compared with the $N_{max}F_2$ values[6] shown in Fig. 2(b) it is found that similar variations occur. Relating these observations to the geomagnetic and solar activity shown in Fig. 2(c), it is found that two of the major deviations in electron content are accounted for by the magnetic storms occurring on March 26–30 and April 9–10. However, the low value of electron content and $N_{max}F_2$ observed on April 3 does not appear to correlate with any unusual geomagnetic activity.

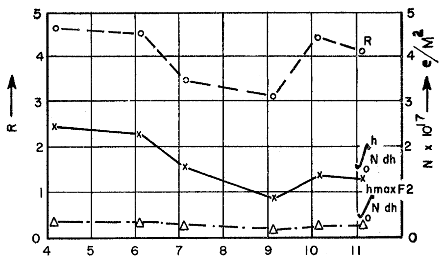

Fig. 1—Electron content, electron content below $h_{max}F_2$ and electron distribution ratio during the pre-dawn period.

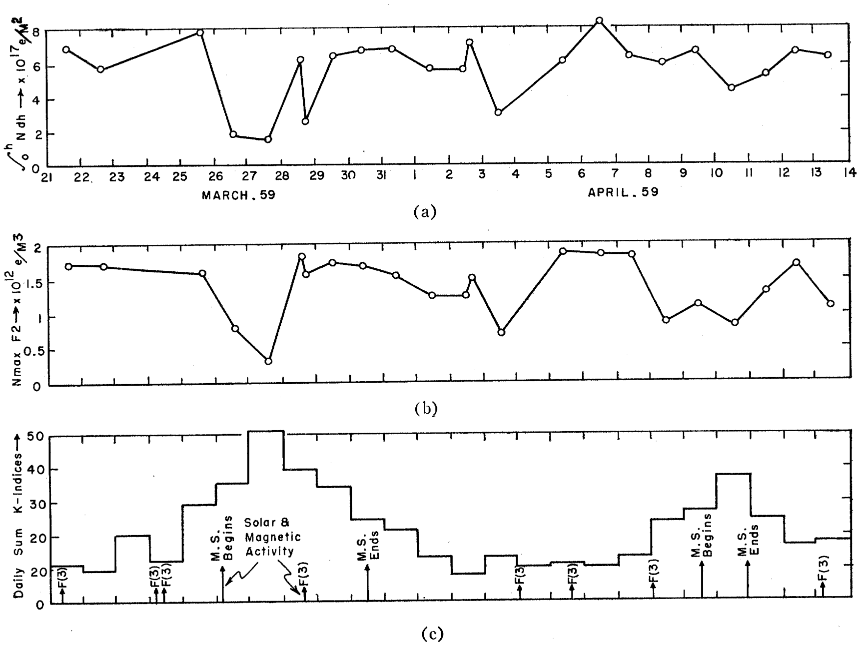

Fig. 2—Correlation of electron content and $N_{max}F_2$ with solar and magnetic activity. (a) Electron content. (b) $N_{max}F_2$ electron density. (c) Daily sum K-indices and solar flares.

T. G. HAME
W. D. STUART
Antenna Lab.
Dept. of Elec. Engrg.
Ohio State University
Columbus Ohio

[2] "Electron Integral to h_{max}," Soundings Research, Sun-Earth Relationships Section, Radio Propagation Physics Div., Nat'l. Bur. Standards, Boulder, Colo. (Private communication.)

[3] S. J. Bauer and F. B. Daniels, "Ionospheric parameters deduced from the Faraday rotation of lunar radio reflections," *J. Geophys. Res.* vol. 60, p. 439; 1958.

[4] J. V. Evans, "The measurement of the electron content of the ionosphere by the lunar radio echo method," *Proc. Phys. Soc. (London)*, vol. 69, pp. 963; 1956.

[5] J. V. Evans, "The electron content of the ionosphere," *J. Atmos. Terr. Phys.*, vol. 11, p. 259; 1957.

[6] "Detailed Values of Ionospheric Characteristics and F-plots for Washington," Central Radio Propagation Lab., Nat'l. Bur. Standards, Boulder, Colo.; March and April, 1959.

Maximum Avalanche Multiplication in *p-n* Junctions*

It has been shown that the rate of build-up of current in avalanche devices (avalanche transistors, 4-layer diodes, etc.) depends upon the value of the multiplication factor in the junctions exhibiting avalanche multiplication.[1-3] To obtain a rapid build-up of current, it is necessary to bias the junction so that M is as large as possible, where

$$M = 1/[1 - (V/V_B)^n],$$

V the reverse voltage across the junction,

V_B the breakdown voltage,

n a number (approximately 3) depending upon the type of material and the impurity concentration.[4]

It is therefore important to know whether there is a limit to the value of M which can be obtained in a practical situation, and what bias conditions are necessary to obtain the maximum M.

The purpose of this note is to obtain, from thermal considerations alone,[5] the following:

1) M_{max}, the maximum value of M that can be realized for a given *p-n* junction, and
2) I_{opt}, the bias current which should be used to obtain M_{max}.

The results of the analysis show that

1) at a given ambient temperature I_{opt} varies inversely with the breakdown voltage V_B, and
2) M_{max} is proportional to the ratio of optimum bias current to thermally generated current with the junction temperature equal to the ambient temperature.

For example, a germanium junction with a breakdown voltage of 42 volts, a thermally generated current of 5 microamperes at the ambient temperature, and a temperature coefficient of 0.5×10^3 degrees C/watt, has M_{max} of approximately 40 and I_{opt} of approximately 0.54 ma.

A simplified biasing scheme is shown in Fig. 1. In this case, the *p-n* junction might be the collector junction of an avalanche transistor in a pulse circuit. The reverse bias current is considered to be the result, in the junction, of the avalanche multiplication of thermally generated carrier pairs. Thus, $M = I/I_s$, where I_s is the thermally generated current. Qualitatively, the following

* Received by the IRE, February 23, 1960; revised manuscript received, April 13, 1960.
This work was done at Stanford Electronics Labs., Stanford, Calif., under Contract Nonr 225(24), NR 373 360.

[1] W. Shockley and J. Gibbons, "Current build-up in semiconductor devices," PROC. IRE. vol. 46, pp. 1947–1949: December, 1958.

[2] W. Shockley and J. Gibbons, "Theory of Transient Build-up in Avalanche Transistors," presented at AIEE Conference, Pittsburgh, Pa. Paper No. 58-1249; September 10, 1958.

[3] D. J. Hamilton, J. Gibbons, and W. Shockley, "Physical principles of avalanche transistor pulse circuits," PROC. IRE, vol. 47, pp. 1102–1109; June, 1959.

[4] S. L. Miller, "Avalanche breakdown in germanium," *Phys. Rev.*, vol. 99, pp. 1234–1241; August 15, 1955.

[5] D. J. Hamilton, "A Theory for the Transient Analysis of Avalanche Transistor Pulse Circuits," Stanford Electronics Labs., Stanford, Calif., Tech. Rept. No. 1701-1; June 15, 1959.

reasoning is helpful in visualizing the existence of a maximum value of M:

As the bias current I is increased from zero, the device dissipation will at first be very small, and I_s will remain essentially constant at its ambient temperature value. The multiplication M thus increases with I. As I is made still larger, the dissipation becomes important because I_s begins to increase. Finally the percentage increase of I is even less than the percentage increase caused in I_s by the rise of junction temperature due to dissipation. A further increase of I causes a reduction of M.

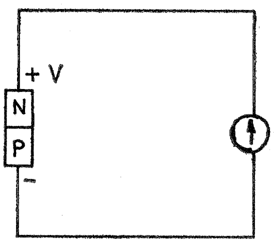

Fig. 1—Equivalent biasing circuit for p-n junction in avalanche operation.

To obtain a quantitative estimate of $M_{\max}$ and I_{opt}, the following approximations are made:

1) All of the current through the junction results from the avalanche multiplication of thermally generated current in the junction. (This precludes surface and other extraneous leakage currents.)
2) It is assumed for convenience that $M_{\max}$ will be greater than 10. Thus, for values of $n \geq 3$, the reverse voltage will be within a few per cent of V_B. The power dissipation of the junction is then approximated by V_BI.
3) The junction temperature rise above ambient is C degrees centigrade per watt dissipation.

The thermally generated current in a junction is

$$I_s = F \exp(-E_G/kT)$$

where E_G is the energy gap between conduction and valence bands, k is Boltzmann's constant, and T is the junction temperature in degrees Kelvin. In reality, F is a function of temperature, but we shall assume that the temperature variation of $\exp(-E_G/kT)$ masks that of F so that in the temperature range of interest, F may be considered constant.

Denoting the ambient temperature by T_a, we may write

$$T = T_a + CV_BI$$

and

$$F = I_{ta} \exp(E_G/kT_a)$$

where I_{ta} is the thermally generated current with the junction temperature equal to the ambient temperature. Thus

$$I_s = I_{ta} \exp\left[\frac{E_G}{kT_a[(T_a/CV_BI) + 1]}\right].$$

We make the additional approximation that $(T_a/CV_BI) \gg 1$. The multiplication factor is then given by

$$M = (I/I_s) = \frac{I}{I_{ta}\exp(E_GCV_BI/kT_a^2)}.$$

Setting $\partial M/\partial I = 0$, we obtain

$$I_{\text{opt}} = (kT_a^2)/(E_GCV_B) \tag{1}$$

and

$$M_{\max} = (I_{\text{opt}})/(I_{ta} \exp 1). \tag{2}$$

It should be emphasized that this analysis was based on the assumption that there were no currents other than the avalanche-multiplied, thermally generated current in the junction. If other currents exist which contribute to the dissipation but not to the avalanche process, the value of $M_{\max}$ will be decreased.

Douglas J. Hamilton
Applied Research Laboratory
University of Arizona
Tucson, Ariz.

An Improvement in the Use of "Piecewise Approximations to Reliability and Statistical Design"*

When a functional relation $T = T(X_1; X_2, X_3, \cdots, X_n)$ is given,[1] and if one is interested in finding the probability of the output T at its near extreme value, then instead of expanding the function near central value by Taylor series, more accurate results will be given if the expansion is carried out at the end point. This amounts to calculating $a_1, a_2, \cdots, a_n$ by substituting the values of $(X_{1e}, X_{2e}, X_{3e}, \cdots, X_{ne})$ which give the extreme value of T, say T_e.

The value of b_i should be obtained from

$$b_i = \frac{a_iX_{ie}}{T_e}.$$

The percentages which are normally expressed with respect to mean value X_{i0} should now be modified with respect to X_{ie}. They will be denoted by p_i.

In relation

$$\xi = \xi_1 + \xi_2 + \cdots \xi_n,$$

$\xi_1, \xi_2 \cdots \xi_n$ and ξ are all distributed from 0 value.

If the variables are uniformly distributed, then the density function of ξ_i is $f_i(X)$, where

$$f_i(X) = 0 \qquad X < 0$$

$$f_i(X) = \frac{1}{A_i} \qquad 0 \leq X \leq A_i$$

$$A_i = p_i \times b_i.$$

The characteristic function of $f_i(X)$ is $\phi_i(t)$, where

$$\phi_i(t) = \frac{1}{A_i}\left[\frac{1}{jt} - \frac{e^{-jtA_i}}{jt}\right].$$

Here the characteristic function is defined, just as the Fourier transform. The characteristic function of output density function

$$\phi(t) = \frac{1}{A_1A_2\cdots A_n}\left[\frac{1}{jt} - \frac{e^{-jtA_1}}{jt}\right] \cdot\left[\frac{1}{jt} - \frac{e^{-jtA_2}}{jt}\right]\cdots\left[\frac{1}{jt} - \frac{e^{-jtA_n}}{jt}\right]$$
$$= \frac{1}{A_1A_2\cdots A_n}\frac{1}{(jt)^n} + \cdots + C_i\frac{1}{(jt)^n}e^{-jtX_i}\cdots,$$

where $X_i = \sum A_i$ are taken one, two, three $\cdots$ etc., at a time and arranged in increasing order of magnitude.

The characteristic function of cumulative density function is

$$\phi(T) = \frac{1}{A_1A_2\cdots A_n}\left[\frac{1}{(jt)^{n+1}} + \cdots C_i\frac{1}{(jt)^{n+1}}e^{-jtX_i}\cdots\right].$$

The probability of output being between extreme end value and a limiting percentage value X_p is given by

$$P(X \leq X_p) = \frac{1}{A_1A_2\cdots A_n}\frac{1}{(n)!}[(X_p)^n + \cdots C_i(X_p - X_i)^n + \cdots C_k(X_p - X_k)^n],$$

where $X_{k+1} \leq X_p \leq X_k$.

K. G. Ashar
IBM Corp
Product Dev. Lab
Poughkeepsie, N. Y

* Received by the IRE, November 23, 1959.

[1] H. J. Gray, Jr., "An application of piecewise approximations to reliability and statistical design," Proc. IRE, vol. 47, pp. 1226–1231; July, 1959.

Modification of Pulse Amplifier Output Stages, Improving Their Response to Negative Edges*

Many pulse amplifiers use as an output stage a conventional cathode follower (Fig. 1), which is usually included into the feedback loop stabilizing the amplifier characteristics.

The main disadvantage of this kind of output stage is its slow response to negative-going pulse edges of short rise time. This well-known effect is because of the valve's being capable of supplying only the charging current for C_{out}, the charging time-constant

* Received by the IRE, April 6, 1960. This work has been carried out under the auspices of the Scientific Department, Ministry of Defense, Israel.

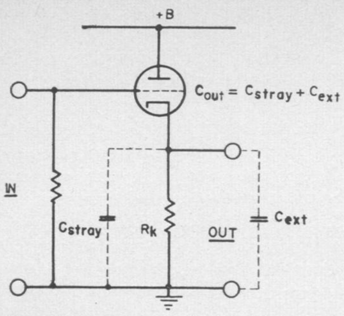

Fig. 1—Conventional cathode follower.

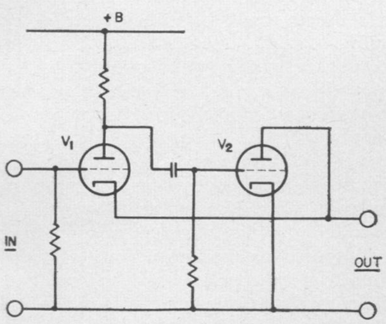

Fig. 2—Simplified White cathode follower.

being approximately $(1/g_m)C_{\text{out}}$. The discharge of C_{out} depends solely on the cathode resistor R_K and is accordingly considerably slower.

The "White Cathode Follower (WCF)" (Fig. 2) provides a well-known solution to this problem.[1] It is essentially a class *AB* push-pull stage with unity gain, providing C_{out} with a charging path through V_1 and a discharging path through V_2. However, the WCF has its drawbacks:

1) It requires an additional valve.
2) Means have to be provided to prevent V_1 from bottoming when it draws heavily on the *HT*, at large input pulses.[2]
3) Its transfer function exhibits two poles in the complex frequency plane, as compared with the single pole of the conventional cathode follower. Thus, special measures have to be taken to maintain monotonic response if one wishes to include the WCF into the feedback loop of an amplifier.[3]

A simple way of providing C_{out} with a discharge path and at the same time avoiding the above enumerated drawbacks is described below. Fig. 3 shows the simplified circuit diagram of a 3-valve feedback loop which is being used in the Model 302A linear

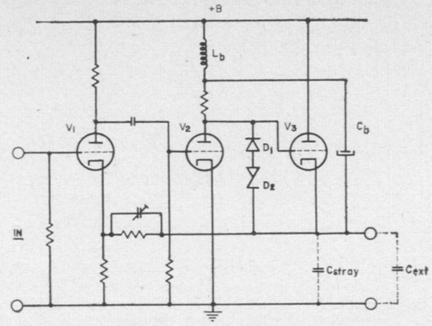

Fig. 3—Three-valve feedback loop. L_b and C_b are a bootstrapping arrangement.[2]

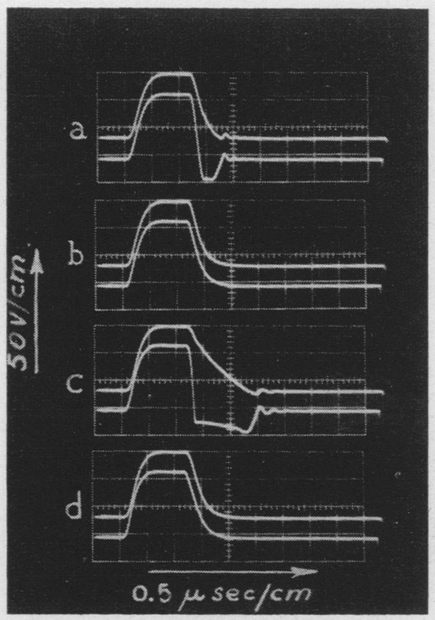

Fig. 4—Wave shapes in amplifier of Fig. 3. Upper traces—output; lower traces—anode of V_2. (a) and (e) before modification, (b) and (d) after modification.

amplifier.[3] The modification introduced is the addition of a Zener diode (D_2) and a high-voltage silicon diode (D_1) in series between the plate of V_2 and the cathode of V_3.

Fig. 4 illustrates the operation of the amplifier under four different conditions, by showing the pulse shapes at the output (upper trace) and at the anode of V_2 (lower trace), for positive input pulses of 0.2-μsec leading and trailing edges. At rise times of this order of magnitude, the detrimental effect of the output capacitance on the negative edge of the output pulse is already considerable.

The operation prior to modification and without external loading is explained with the aid of Fig. 4(a). The slow discharge of the output capacitance causes V_3 to be driven into cutoff and prevents the waveform at the anode of V_2 from being fed back to the cathode of V_1, thereby opening the feedback loop. The ensuing high forward gain causes V_2 to draw current heavily and to lower its anode potential sharply, thereby driving V_3 further into cutoff. After C_{out} discharges sufficiently to allow V_3 to conduct, the feedback loop closes again. However, because of the low g_m of the valve near cutoff, the output time constant $[(1/g_m)C_{\text{out}}]$ is considerably larger than under normal conditions. The resulting increased phase lag is the cause of the non-monotonic transient observed at the end of the pulse.

The influence of additional external loading is evident from Fig. 4(c). The larger time constant $C_{\text{out}}R_K$ considerably lengthens the discharge time, and hence the cutoff period.

This analysis emphasizes the need to discharge C_{out} quickly, as well as to maintain the g_m of V_3 above the minimum value which is required for monotonic response. A review of the operation of the amplifier brings out the point that during the time C_{out} is to be discharged, V_2 draws a heavy current. Now, introduction of a Zener diode (D_2) as indicated in Fig. 3, enables C_{out} to discharge through V_2 as soon as the Zener diode breaks down because of the inability of the cathode voltage to follow the sharp drop in the grid voltage.

During the breakdown period of the Zener diode, the output capacitance is effectively parallel to the one at the anode of V_2, so that the number of poles at the feedback loop in the complex frequency plane is decreased by one (their number would be increased by one were a WCF used for improvement of the performance). This fact insures monotony of response during the breakdown period.

A proper choice of the breakdown voltage of the Zener diode will limit the grid cathode voltage of V_3 to such a value that its g_m will be sufficiently high to maintain monotonic response after the Zener diode recovers from conduction.

Fig. 4, (b) and (d) are the replicas of (a) and (c), respectively, after modification. The negative edges of the pulses are quite similar to the positive ones. The heavy capacitive loading, shown in Fig. 4(d), causes only very slight lengthening of the rise times of both edges.

The power rating of the Zener diode should be adequate to cope with the discharge currents under the highest PRF's expected.

The high-voltage silicon diode (D_1) decreases the effective capacitance of the Zener diode and protects the latter from occasional high forward current surges which may be caused by on-off switching or by pulling out V_2 or V_3.

Conclusion

Pulse amplifiers of the type shown in Fig. 3 may be easily modified to provide a better negative edge response, at the cost of two diodes. In case RC coupling is used, it should first be replaced by direct coupling. For large capacitive loads, it might be advisable to use, for both V_2 and V_3, a power valve in order to equate the maximum available charging and discharging currents.

I. Bar-David
Scientific Dept.
Ministry of Defence
Israel

[1] Moody, Howell, and Taplin, "The Chalk River pulse amplitude analyzer," *Rev. Sci. Instr.*, vol. 22, pp. 555–558; August, 1951.

[2] E. Fairstain, "Nonblocking double line linear pulse amplifier," *Rev. Sci. Instr.*, vol. 27, pp. 472–482; July, 1956.

[3] A. F. Fischmann-Arbel and I. Bar-David, "A method of linear pulse amplifier design," to be published in *Nuclear Instruments and Methods.*

A Proposed Technique for F-Layer Scatter Propagation*

The continuing need for reliable radio circuits over great distances is becoming ever more acute. The purpose of this note is to suggest a method that may be useful in providing reliable ionospheric circuits at frequencies above the classical F_2 MUF.

In what follows, the term F_2 *MUF* will be used to specify the *conventionally calculated* maximum usable frequency of the F_2 region of the ionosphere. It is equal, numerically, to the critical frequency at vertical incidence multiplied by the secant of the angle between an incident ray and the normal to the ionosphere.[1]

Since the technique to be described attempts to make use of frequencies above the F_2 MUF, it may be considered in one sense a form of "*F*-layer scatter" propagation. Unfortunately, the term "scatter" has been used in recent years to describe a multiplicity of apparently unrelated physical phenomena. For this reason, a brief description is presented below of the scattering mechanism to be considered in this paper.

A physical model, first proposed by M. L. Phillips,[2,3] can be used to represent the reflection, either total or partial, of radio waves by the ionosphere. It is hypothesized that the ionosphere is made up of a vast number of irregularly ionized volumes. Each of these innumerable volumes will have associated with it a value of MUF corresponding to the electron density within the volume. It would be reasonable to assume, then, that the distribution of MUF values would vary in a Gaussian manner about the conventionally calculated MUF, *i.e.*, the value used in the operation of ordinary ionospheric circuits. The true distribution, of course, is somewhat skewed, but since the present discussion deals only with frequencies above the MUF (the modal value of the distribution), the lower percentiles are of little interest. It is practicable, therefore, to consider that the distribution of elemental MUF's follows a true Gaussian distribution. Fig. 1 represents such a distribution.

The conventionally calculated path MUF is represented by the vertical line intersecting the central value of the distribution. The curve represents the distribution of actual elemental MUF's above and below that value. The frequency designated by F_1 represents a typical operating frequency of a high-frequency, point-to-point circuit. Such a frequency is lower than most of the elemental MUF values of the F_2 region. Consequently, most of the ionized volumes will be effective in reflecting the signal back to earth. Frequency F_2, on the other hand, is higher in frequency than most of the MUF values, and only a small percentage of these are capable of reflecting the incident energy

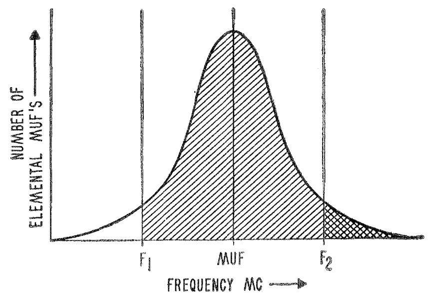

Fig. 1—Assumed distribution of elemental MUF-values as a function of frequency.

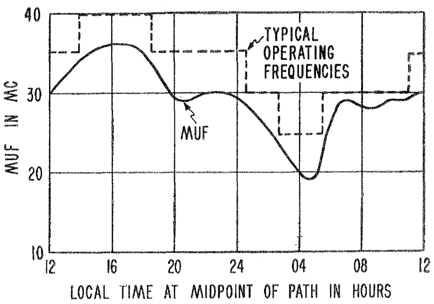

Fig. 2—Typicalfrequency changes required to employ the F_2-Layer scatter mechanism.

back to earth. It is only necessary, then, to determine the standard deviation σ of the distribution, in order to relate this physical model to *F*-layer reflection phenomena at frequencies above the F_2 MUF.

A curve has been developed[2] experimentally which relates the scatter loss L to X/σ where X represents the number of megacycles by which the operating frequency exceeds the F_2 MUF, and σ (in megacycles) is defined as above. A few corresponding values are given below to illustrate orders of magnitude.

X/σ	L (decibels)
0	3
1	8
2	17
3	29
4	45
5	66
6	89

The values of L given above must be added to the path loss that would be encountered if the system were operating at an optimum frequency slightly below the MUF.

Phillips has deduced values of σ from 1 to 2 mc for ionospherically quiet conditions in the eastern part of the United States. Values to perhaps 4 mc pertain to ionospherically-disturbed conditions.

With this information in hand, it occurred to the authors that a practicable radio circuit might be established between two points at frequencies above the conventional F_2 MUF. Because of the diurnal, seasonal, and cyclical variation of the MUF, however, any such technique would require a frequency changing capability in order to prevent the operating frequency from exceeding the MUF by too great a margin. On the other hand, it would also be necessary to change frequencies so that the system would never encroach upon other systems in use below the MUF. The dashed line of Fig. 2 illustrates the way in which the operating frequency might be varied diurnally in order to make use of the F_2-layer scatter mechanism.

The system would operate much the same as a conventional below-the-MUF system, except for the operating frequency, which would always exceed the F_2 MUF. In this way, a new group of frequencies would become available for ionospheric propagation without the inherent disadvantages associated with *D*/*E*-layer systems.

An *F*-layer system, for example, should not be susceptible to interference (or bandwidth limitations) from the motion of ionized meteor trails. It is well known[4] that such trails occur at heights from 80 to 120 km above the earth, heights corresponding roughly to the *E* layer. The incidence of ionized meteor trails is negligible at *F*-layer heights.

Another factor which might affect the bandwidth of an *F*-layer scatter system is the motion of charges existing within the ionosphere itself. It has been shown[1] that the fast fading rate of an ionospheric signal increases by a factor of 4 or 5 at the transition from "normal layer" to *F*-layer scatter propagation. This phenomenon might be attributable to a more rapid rate of drift or diffusion of the electrons in the ionosphere. It is known[5] that this velocity is of the order of 2 or 3 msec at the lower HF frequencies. It will be somewhat higher for scatter signals, but it is not likely that the velocity would approach the many thousands of meters per second necessary to produce interference to frequency division multiplex systems.

In the system design of an *F*-layer scatter circuit, the path should be chosen to have a length near the maximum limit of single-hop propagation. The MUF for such a path is near the highest possible value. This permits the use of frequencies well above the range that is useful for conventional point-to-point circuits at any given time, in any particular part of the world.

It should be pointed out, of course, that the appropriate values of σ may vary considerably with geomagnetic latitude, longitude, time of day, period in the sunspot cycle, etc. Considerable work must be done to determine that suitable values do, in fact, exist for a particular path. In this regard, the prevalence of spread-*F* conditions in equatorial regions will result in higher values of σ for a large fraction of the time, especially during the period of low early morning MUF's during the low portion of the sunspot cycle. During 1944, for example, the Maui and Christmas Island ionograms recorded severe spread *F* to exist over 50 per cent of the time during the hours in question. As a result, σ would have relatively high values when the F_2 MUF is lowest, permitting the use of relatively higher operating frequencies at such times.

W. C. Vergara
J. L. Levatich
Advanced Res. Dept.
Bendix Radio Div.
The Bendix Corp.
Towson, Md.

* Received by the IRE, April 6, 1960.

[1] J. A. Ratcliffe, "The Magneto-Ionic Theory and Its Applications to the Ionosphere," Cambridge University Press, Cambridge, Eng., p. 160: 1959.

[2] M. L. Phillips, "F-Layer Radio Transmissions on Frequencies Above the Conventionally Calculated MUF," a portion of "Project Earmuf, Final Report," Signal Corps Contract DA-36-029-SC-72802, pp. 138–162; September, 1958.

[3] M. L. Phillips, M.I.T. Lincoln Lab., Lexington, Mass.; report now in preparation.

[4] B. Lovell and J. A. Clegg, "Radio Astronomy," John Wiley and Sons, Inc., New York, N. Y., ch. 10; 1952.

[5] R. W. E. McNicol, "Fading of radio waves of medium and high frequencies," *Proc. IEE*, vol. 96, pt. III, pp. 517–524; October, 1949.